UiT The Arctic University of Norway

Faculty of Science and Technology, Department of Physics and Technology

Raman-spectroscopy and of optically trapped nanoparticles

Ivan Mikheev

Master's thesis in Physics FYS-3900-1 November 2022]

Abstract

The present work begins a large layer of experiments on the study of Raman radiation from extracellular vesicles. It is a promising method that provides unique information about the global biomolecular composition of a single vesicle or a small number of vesicles. Two physical phenomena are present in this work, Raman scattering and optical trapping.

In Raman scattering, the scattered radiation depends on the molecular structure of the scatterer. The amount of energy that is lost or gained in such interactions is determined by molecular vibrations and oscillations. By collecting and analyzing the spectra of the scattered light, the structure of a molecule can be identified.

Objects represented as small dielectric spheres interact with the electric field created by the light wave due to the dipole moment induced on the sphere. As a result of the interaction of this dipole with the electric field of the electromagnetic wave, the object moves along the electric field gradient. In addition to the gradient force, the object is also affected by the force caused by the pressure (reflection) of light from its surface. These two effects can be used to trap and control micro- and nanoparticles.

Confocal Raman tweezer microscope has been designed and constructed. A focused laser beam has been used to optically trap polystyrene beads and excite Raman-scattering. The Raman-scattered light has been transmitted to an optical spectrometer. As the PS beads are in a buffer-solution, a considerable Raman-background is present and has to be subtracted. Due to this and the fact that the Raman-scattering is weak, major part of the project is to optimise the signal-to-noise ratio by choosing a good design and experimental testing.

Raman spectra are obtained of nanometer-sized polystyrene particles trapped by a laser tweezer. It provides sufficient sensitivity for the Raman measurement of the trapped nanoparticles. The set-up and allows us to determine their molecular structure.

The presented studies were performed to investigate the validity of Raman tweezer microspectroscopy. This set-up can be used in the future experiments with biological nanoscale particles such as extracellular vesicles.

Table of Contents

1 Introduction

The aim of this master-project was to make a set-up combining a microscope with optical trapping and Raman-spectroscopy and use the set-up for characterisation of polystyrene (PS) beads. The installation should thus be prepared for further use to characterize extracellular vesicles.

Extracellular vesicles (EVs) are bilayer membrane vesicles (30-1000 nm) released from various cells into their surroundings. EVs are considered a mechanism for intercellular communications, allowing cells to exchange proteins, lipids and genetic material [1]. EVs can be important indicators of different conditions of a producing organism, and elevated plasma levels of EVs have been associated with several disease states such as atherosclerosis, diabetes, cancer, arterial cardiovascular diseases and venous thromboembolism [2]. New methods to characterise and analyse EVs are essential to understand the physiological and pathological functions of these vesicles, and to develop new clinical methods involving their use and/or analysis. Raman-spectroscopy can reveal the chemical composition, or 'chemical fingerprint', of a sample. However, owing to the small EV size, acquisition of Raman signals from EVs is very demanding. By combining optical trapping with Raman-spectroscopy, it is possible to collect the Raman-spectrum of a few EVs [3]-[8].

Raman spectroscopy is a spectroscopy technique based on the physical phenomena known as Raman scattering. It determines electromagnetic radiation emitted by rotational and vibrational modes of molecules. It can provide fingerprints of molecular structures and molecules of a sample. A sample, typically, is illuminated by a powerful laser beam to excite the scattering since it is very weak. Then the Raman-scattered light is collected by a high NA objectives and analyzed by a spectrometer. There are three wavelengths detected, one corresponds to the laser line (Rayleigh scattering) and the other two are shifted, called anti-Stokes and Stokes Raman scattering. These two provide information about the molecular structure of the sample. The anti-Stokes spectrum is much weaker than the Stokes spectrum, and it is thus Stokes that is used [9]-[10].

Since the objective of this project is to characterization of nanoparticles, optical trapping technique was chosen as a common method for collecting Raman spectra of such particles. The principal pioneer of optical laser trapping (also known as optical tweezers) is considered to be Arthur Ashkin. in 1970 [11] he successfully used radiation pressure from a continuous laser

source to trap micron-sized particles in stable optical potential wells and in 2018 received the Nobel Prize in Physics. An optical trap is created when a laser beam is brought to a tight focus by use of a high numerical aperture lens. Optical trapping allows levitation of particles above the substrate, which reduces fluorescence and Raman background effects as well as Brownian motion of the un-trapped particles. Therefore, this leads to a reduction of a background signal. Trapping in this way also eliminates the need to immobilise particles to substrates, which could alter the sample's microenvironment. In the current set-up the same laser beam is used for both Raman scattering excitation and optical trapping [12]-[14].

In this master-project, confocal Raman tweezer microscope was designed and constructed. A focused laser beam was used to optically trap PS beads and excite Raman-scattering. The Raman-scattered light was transmitted via an optical fibre to an optical spectrometer. As the Raman-scattering is weak, several design considerations must be taken to get an acceptable signal-to-noise ratio. The signal depends on the power of the laser used, the transmission of the optical system, the spot-size in the focal plane of the microscope objective, and sensitivity of the CCD-camera on the spectrometer. The noise depends on the fluorescence and Raman-background, noise of the CCD-camera, the number of photons and any white light received by the camera. White light could be from side-bands of the laser-emission that are not stopped completely by a laser-line filter. As the PS beads were in a buffer-solution, a considerable Raman-background were present and had to be subtracted. The buffer-solution could also emit fluorescence, depending on the wavelength of the laser. A major part of the project was to optimise the signal-to-noise ratio by choosing a good design and experimental testing.

Analysis of the Raman-spectrum was done with standard methods to find the chemical composition of the PS beads. In the future, the system will be used to characterise EVs from collaborators at the Faculty of Health Sciences.

2 Raman scattering

2.1 Introduction

Raman scattering of light is inelastic scattering of optical radiation by molecules of a substance (solid, liquid or gaseous), accompanied by a noticeable change in the radiation frequency. In contrast to Rayleigh scattering, Raman scattering spectral lines appear in the spectrum of scattered radiation, which are absent in the spectrum of the primary (exciting) light. The number and location of the lines that have appeared is determined by the molecular structure of the substance. This section describes basic physical principles of Raman scattering from the point of view of classical electrodynamics and the quantum theory of radiation.

2.2 Classical theory of electrodynamics

In the classical model, the electric field of light induces a variable dipole moment of a molecule, which oscillates with the frequency of the incident light. And changes in the dipole moment, in turn, lead to the emission of radiation by the molecule in all directions. In the classical model, it is assumed that matter contains charges that can be separated, but are held together by the Coulomb attraction. The formation of a wave at the boundary with matter causes an oscillating separation of these charges. That is, an oscillating electric dipole appears. And it radiates at the oscillation frequency. This radiation is the raman scattering. The expression for the radiation intensity is taken from [15]

$$I = \frac{16\pi^4 \nu^4}{3c^3} \left|\vec{P}\right|^2 \quad (1)$$

where $\vec{P}$ is induced dipole moment, defined as $\vec{P} = \alpha\vec{E}$, α – polarizability of the molecule.

Consider a light wave as an electromagnetic field of intensity $\vec{E}$ with a frequency of oscillations ν_0

$$\vec{E} = \vec{E}_0 \cos(2\pi\nu_0 t) \quad (2)$$

Therefore, for a diatomic molecule placed in this field, the induced dipole moment $\vec{P}$ is written as

$$\vec{P} = \alpha\vec{E}_0 \cos(2\pi\nu_0 t) \quad (3)$$

If the dipole emits according to the classical laws and the initial radiation is polarized, then the scattering is also polarized, if we consider the particles are isotropic. This is Rayleigh scattering, and its intensity is proportional to the mean-square value $\vec{P}$.

In the general case, the polarizability depends on the frequency of the field. Therefore, it will be different for a static field and electromagnetic radiation. Consider the case when α depends only on the normal oscillations of the molecule. If the molecule oscillates with a frequency ν_1, then the displacement of the nuclei x (generalized coordinate) can be written as

$$x = x_0 \cos(2\pi\nu_1 t) \tag{4}$$

where x_0 is the oscillatory amplitude. Let us expand α in a Taylor series, for the small oscillations, in the coordinates of the displacement of the nuclei x near the equilibrium position, it is usually limited by the first term

$$\alpha = \alpha_0 + \left(\frac{d\alpha}{dx}\right)_0 x \tag{5}$$

Substituting expressions (4) and (5) into equation (2), we obtain the following expression for the induced dipole moment:

$$\vec{P} = \alpha\vec{E}_0 \cos(2\pi\nu_0 t) = \alpha_0\vec{E}_0 \cos(2\pi\nu_0 t) + \left(\frac{d\alpha}{dx}\right)_0 x\,\vec{E}_0 \cos(2\pi\nu_0 t)\cos(2\pi\nu_1 t) =$$
$$\alpha_0\vec{E}_0 \cos(2\pi\nu_0 t) + \frac{1}{2}\left(\frac{d\alpha}{dx}\right)_0 x\vec{E}_0 \{\cos[2\pi(\nu_0 + \nu_1)t] + \cos[2\pi(\nu_0 - \nu_1)t]\} \tag{6}$$

The first term describes an oscillating dipole whose radiation frequency is ν_0 (Rayleigh scattering), the second term refers to Raman scattering with frequencies $(\nu_0 + \nu_1)$ (anti-Stokes) and $(\nu_0 - \nu_1)$ (Stokes). Thus, when the molecule is illuminated with monochromatic light of frequency ν_0, as a result of induced electronic polarization, it scatters radiation at both frequency ν_0 and frequencies $(\nu_0 \pm \nu_1)$ (Raman scattering), where ν_1 is the frequency of the molecule oscillations.

2.3 Quantum theory of radiation

The origin of Raman scattering is most conveniently explained within the quantum theory of radiation. According to it, radiation of frequency ν_0 is considered as a flux of photons with energy $h\nu_0$, where h is Planck's constant. In collisions with molecules, photons transmit the

molecules to virtual energy states and then they re-emit photons (scattering) moving back to the initial energy state (Fig. 1). In the case of elastic scattering, they will deviate from the direction of their motion without changing their energy (Rayleigh scattering). But it may also be the case that in the collision there will be an exchange of energy between the photon and the molecule. In this case, the molecule can both acquire and lose a part of its energy in accordance with the rules of quantization: its energy can change by an amount ΔE corresponding to vibrational or rotational energy sublevels, therefore $\Delta E = h\nu_1$, where ν_1 is the frequency of normal molecule oscillations (Fig. 1). In other words, the value of ΔE should be equal to the change in the vibrational or rotational energies of the molecule. If the molecule acquires energy ΔE, then the scattering photon will have energy $h\nu_0 - \Delta E$ and, accordingly, the frequency $\nu_0 - \frac{\Delta E}{h} = \nu_0 - \nu_1$ (Stokes). And if the molecule loses energy ΔE, the scattering photon frequency will be equal to $\nu_0 + \frac{\Delta E}{h} = \nu_0 + \nu_1$ (anti-Stokes).

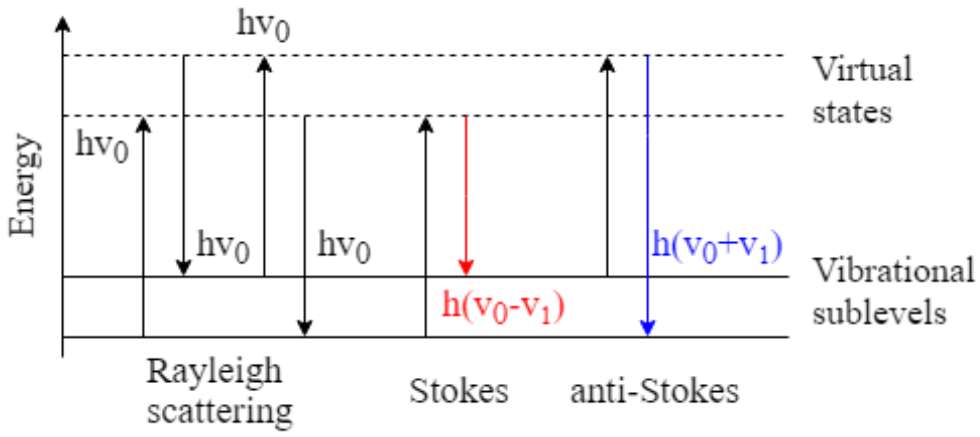

Fig. 1: Jablonski diagram for Raman scattering.

2.4 Empirical laws of Raman scattering

- Spectral satellite lines accompany each line of primary light. The satellites are two groups of lines located symmetrically with respect to the exciting line.
- The frequency shift of satellites relative to the primary line characterizes the scattering substance and is equal to the normal frequencies of molecular vibrations.
- As the temperature rises, the intensity of the anti-Stokes satellites increases rapidly. Since the population of the excited vibrational sublevel increases with increasing temperature [15].

3 Optical trapping

3.1 Introduction

Optical trapping [11] uses a highly focused laser beam to hold and move microscopic and sub-microscopic objects like atoms, nanoparticles and droplets, in a manner similar to tweezers. This section describes how forces of an optical beam act on small particles.

3.2 Rayleigh approximation

Let us consider the case when the characteristic size of the trapped particle is much smaller than the wavelength of light (Rayleigh scattering condition) [16]. Then the particle can be considered as a point dipole in an inhomogeneous electromagnetic field. Lorentz force acting on a charged particle in the electromagnetic field

$$\vec{F} = q\left(\vec{E} + \vec{v} \times \vec{B}\right) \tag{7}$$

where $\vec{v}$ is the velocity of the particle.

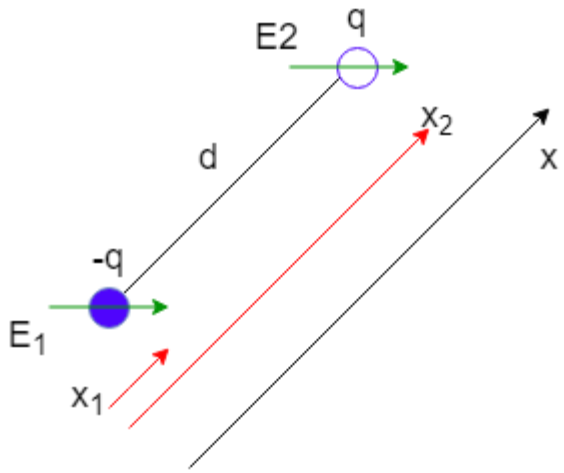

Fig. 2: Dipole in an inhomogeneous electromagnetic field.

The force acting on the dipole is calculated from the sum of the forces acting on separate opposite charges (Fig. 2):

$$\vec{F} = \vec{F}_1 + \vec{F}_2 \tag{8}$$

$$\vec{F} = q\left(\vec{E}_2 - \vec{E}_1 + \frac{d(\vec{x}_2 - \vec{x}_1)}{dt} \times \vec{B}\right) \tag{9}$$

Due to the small distance $\vec{d} = \vec{x}_2 - \vec{x}_1$ between the charges in the dipole, the electric field can be expanded in Taylor series near the first charge:

$$\vec{F} = q\left(\vec{E}_1 + (\vec{d}\nabla)\vec{E}_1 - \vec{E}_1 + \frac{d\vec{d}}{dt} \times \vec{B}\right) \tag{10}$$

Substituting induced dipole moment $\overrightarrow{P} = q\vec{d} = \alpha\vec{E}, \alpha = \varepsilon_0\chi\vec{E}$, where ε_0 is the electric constant and χ is the electric susceptibility

$$\vec{F} = (\vec{P}\nabla)\vec{E} + \frac{d\vec{P}}{dt} \times \vec{B} = \alpha\left[(\vec{E}\nabla)\vec{E} + \frac{d\vec{E}}{dt} \times \vec{B}\right] = \alpha\left[\frac{1}{2}\nabla E^2 + \frac{d}{dt}(\vec{E} \times \vec{B})\right] \tag{11}$$

The second term in the last equality is the time derivative of the quantity, which is connected through a constant factor with the Poynting vector, which describes the power of the radiation passing through the unit area. Assuming that the laser power is independent of time, the derivative of this term is zero, and the force is written as

$$\vec{F} = \alpha\frac{1}{2}\nabla E^2 \tag{12}$$

The square of the electric field is equal to the intensity of the beam as a function of coordinates. Therefore, the result indicates that the force acting on the dielectric particle in the point-dipole approximation is proportional to the gradient of the beam intensity. In other words, the force described here causes the particle to be attracted to the region with the highest intensity. In fact, the force arising from light scattering depends linearly on the intensity of the beam, the cross section of the particle and the refractive index of the medium in which the trap is located (for example, water), works against the gradient force in the axial direction of the trap, causing the equilibrium position to shift slightly down from the position of the maximum intensity.

4 Literature review

4.1 Introduction

In this section we reviewed several articles on "Optical trapping and Raman tweezer microspectroscopy" topic and also one commercial setup form Thorlabs . Though, the method is only used as a tool for further research in the reviewed articles, we focused on experimental setups, materials and methods used.

4.2 S. Kruglik et al. Raman tweezers microspectroscopy of circa 100 nm extracellular vesicles [3]

In this work, authors described in detail the method of Raman tweezers microspectroscopy (RTM) for EV characterization, in the nanoscale domain, with particles' size ranging from approximately 50 nm to a few hundreds of nm.

Raman tweezers microspectroscopy.

They recorded raman spectra using a home-built RTM setup. Near-infrared (NIR) excitation at 780 nm (approximately 100 mW at the sample position) was provided using a continuous-wave Ti-Sapphire laser (Spectra Physics model 3900S) pumped by an Ar-ion laser (Spectra Physics Stabilite 2017). Raman scattering was excited using a long-working-distance water-immersion infinity-corrected objective (Olympus LUMFL, M = 60x, NA = 1.1) directly plunged into the droplet (∼100 µl) of the water buffer solution containing bioparticles of interest. Kruglik and the team chose an upright configuration because of several advantages. First, sedimentation of particles or debris from the sample solution during the experiment did not interfere with the optical path; second, the contribution to the overall Raman signal from any material within the optical path was eliminated (e.g., stage slide, coverslip, or matching fluid) or reduced to a strict minimum. In the experiments, the focal point (optical trap) was located inside the sample droplet, approximately 2 mm above the stage slide made of CaF2.

Authors collected raman signal in a backscattering geometry, spectrally filtered off with a matched combination of beamsplitter and long-pass filter (Semrock RazorEdge "U"), dispersed by a 500 mm focal length spectrograph (Acton SpectraPro 2500i) with a 400 mm−1 grating optimized for 850 nm, and registered by a back-illuminated NIR CCD detector (Princeton Instruments SPEC-10 400BR/LN) cooled to 140° K using liquid nitrogen.

A “semi”-confocal configuration was implemented using a 50 µm slit with a height of 10 mm at the spectrometer entrance, together with a 75 mm achromatic focusing lens, where the effective volume of Raman signal collection can be estimated as a cylinder. Because the Raman signal from nanosized bioparticles is extremely weak therefore true confocal signal collection using a diffraction-limited pinhole is problematic, as it substantially reduces the throughput of the detection pathway.

The spectral resolution of our RTM setup with a 50 µm spectrometer slit width was about 5 cm^{-1}. Frequency calibration was performed using Raman lines of toluene with an absolute accuracy of ±2 cm−1 and a relative frequency position accuracy of ±1 cm^{-1}. Spectra were acquired using the WinSpec software; further data treatment was performed with the IgorPro for Windows software package. In this work, for Raman kinetics measurements on the basis of spectral band areas, an additional step of automatic background correction using spline functions was introduced.

Cryogenic transmission electron microscopy (Cryo-TEM).

Cryo-TEM images of the studied samples were obtained. A 4 µl droplet of an aqueous suspension of bioparticles with the highest available particle concentration was deposited onto a Quantifoil® holey carbon grid. Excess liquid on the grid was absorbed with filter paper. Then, using a specially designed appliance, the grid was rapidly plunged into liquid ethane to form a thin homogeneous vitreous ice film. The vitrified sample was then placed in a Gatan 626 liquid-nitrogen cooled cryo-holder, transferred into the side microscope entry, and studied at low temperature (−180 °C). Cryo-TEM images were recorded with a 2k × 2k Gatan Ultrascan 1000 CCD camera using an LaB6 JEOL JEM2100 transmission cryo-electron microscope operating at 200 kV. Images were taken with a JEOL low-dose system to protect the thin vitreous ice film from any irradiation before imaging and to reduce the irradiation during image recording.

4.3 Irène Tatischeff et al. Fast characterisation of cell-derived extracellular vesicles by nanoparticles tracking analysis, cryo-electron microscopy, and Raman tweezers microspectroscopy [4].

Irène was working with Sergei from the previous article. So she used basically the same RTM setup. But it is noteworthy to go through her method of raman spectra acquisition and data treatment.

Author stated that the informative signal from the vesicles in the sample volume arised as additional spectral features appearing on top of the PBS Raman spectrum, as soon as the vesicles are trapped at the focus of the laser beam. The process of vesicles trapping is rather stochastic and the resulting Raman signal depends on various parameters such as the vesicle molecular composition, size, concentration, density and the laser power.

Before the study on EVs, they performed a preliminary investigation of the particularities of the RTM signal using a suspension of model DOPC liposomes of various known sizes, solutions of bovine serum albumin (BSA) and calf-thymus DNA, as a function of sample concentrations. Briefly, their setup was capable of trapping and detecting a very weak but distinguishable Raman signal from a single empty liposome of 200-nm size, while several (~5-10) trapped vesicles in the 50-200 nm size range are required for a reliable liposome characterization.

Raman spectra were acquired every 3 seconds (for D. discoideum EVs) or every 6 seconds (for urine exosomes) during a sequence of 20 consecutive measurements: this was one ‘‘experimental set’’. Measurements kept going until the event of optical trapping of at least several vesicles in the focus of the microscope objective (so-called ‘‘vesicle set’’); after this event, a few more experimental sets were sequentially acquired for a better signal averaging. The transition from one vesicle set to another was accomplished by blocking the laser beam for 10 seconds, the trapped particles in the measurable volume being then exchanged by Brownian motion.

The process of data treatment consisted of the following successive steps:

a. All of the recorded raw Raman spectra were visually inspected and properly selected, to eliminate the spectra without (or with very minor) vesicles contribution, with high background and poor quality.

b. The selected raw Raman spectra were averaged and normalized on the water bending band around 1,640 cm^{-1}.

c. The contribution from PBS was subtracted.

d. The resulting spectra were smoothed by 2 (for D. discoideum EVs) or 3 (for urinary exosomes) adjacent pixels, to minimize the etaloning effect in back-illuminated NIR-CCD detector.

e. In some cases, a slowly changing background originating from strong stray Rayleigh scattering was subtracted in using the cubic spline interpolation from Igor Pro software.

4.4 Katsuhiro Ajito, Keiichi Torimitsu. Single Nanoparticle Trapping Using a Raman Tweezers Microscope [23].

A commercial Raman microprobe spectrometer (Ramascope, Renishaw Ltd.), used in this work, contained a high-power NIR laser, an optical microscope, holographic notch filters (HNFs), a single-grating polychromator, and a charge-coupled device (CCD) camera was specially modified for NIR laser light. The excitation light source was a continuous-wave, single-frequency Ti: sapphire ring laser (Titan-CW, Schwartz Electro-Optics) tuned to 730 nm in the TEM00 mode. The pump source for the Ti :sapphire ring laser was the 532- nm line (pumping power: 5 W) of a solid-state visible continuous-wave laser (Millenia, Spectra-Physics Lasers). The laser beam, 120 mW, passed through the optical microscope (BH-2, Olympus) and was focused onto the sample using the objective lens mounted on the optical microscope. The objective lens had 100x magnification with a numerical aperture of 1.25, which was immersed in oil with a refractive index (N_D) of 1.52 at 296 K. The 0.25-m single polychromator was fitted with a 1200 mm^{-1} grating and was used to disperse the scattered light. The dispersed light was then focused onto a CCD camera (02- 06-1-225, Wright Instruments) that contained a Peltiercooled slow-scan 384 3 576 CCD chip maintained at 200 K. The two-slit confocal arrangement used for Raman measurement24,25 was adjusted to the focal spot size of the laser beam, about 1 μm. The nanoparticle sample used in the measurement was a polystyrene latex bead about 42 nm in diameter (Stadex, JSR), which had an N_D of 1.59 at 293 K. Beads were dispersed in deionized water (Milli-Q, Millipore) at a concentration of 10^{-4}% wt (1 ppm), fixed in the glass cell, and then covered with a glass coverslip inserted between the oil-immersed objective lens and the stage.

4.5 Mu-ying Wu et al. Stable optical trapping and sensitive characterization of nanostructures using standing-wave Raman tweezers [24].

A single laser beam at 780 nm from a semiconductor laser (TEC-300–0780–0500, Sacher Lasertecknik Inc.) coupled into a single-mode optical fiber was used both for Raman spectroscopy excitation and optical trapping. The laser source had a frequency bandwidth <1 MHz and a narrow band-pass filter (LL01–780–12.5, Semrock Inc.) was used to spectrally purify the laser beam. A pair of lens (L1 and L2) were used to expand the laser beam to fill the exit pupil of the objective with high numerical aperture (NA). A half-wave plate was used to

change the polarization direction of the incident laser beam. The laser beam was introduced into the objective (100x, 1.3NA, Nikon) of an inverted microscope (TE-2000S, Nikon) through a dichroic mirror D1 (LPD02–785RU-25, Semrock Inc.), a pair of tube lens (L4 and L5), and a hot mirror D2 to form single-trap optical tweezers.

The tightly focused laser beam was reflected by a planar dichroic mirror (>98% reflection for 750–1100 nm and >90% transmission for 400–700 nm) and interfered with the incident beam to form a standing wave optical trap (SWOT) in a sample chamber, which was made of a bottom glass coverslip and the reflecting dichroic mirror separated by a 50-μm spacer. When the focus of the objective was moved onto the reflecting surface or a distance <0.5 μm from it, the reflected beam was spatially matching the incident focused beam such that a stable SWOT was formed at the first node from the mirror, which could be sharply imaged by the microscope. A slight adjust of the microscope focus could transport the trapped particle in the second node to the first node. On the other hand, when the focus of the objective wass adjusted to a distance >10 μm below the reflecting surface, the reflected beam was too diverging to interfere with the incident focused beam such that the trapping was dominant by a single-beam optical tweezers. Therefore, by adjusting the focus distance of the objective, a standing-wave optical trap could be changed to a single-beam optical tweezers, and vice versa.

Raman scattering light from a trapped nanoparticle was collected with the same objective lens, passes through a dichroic mirror and a long-pass filter (LP02–780RU-25, Semrock Inc.), and then focused onto the entrance slit of an imaging spectrograph (Triax 320, Horiba Scientific), which contained a CCD detector (PIXIS 100BR, Princeton Instruments) to record the Raman spectra of the trapped particles. In order to reject the out-of-focus light from the specimens, five pixels of the CCD detector were binned and the entrance slit of the spectrograph was set as 100 μm, corresponding to spatial filtering with a confocal pinhole. The bright-field or differential interference contrast (DIC) images of a trapped nanoparticle is illuminated with a lamp and recorded with a video CCD camera. The background spectrum was collected without a nanoparticle in the trap and subtracted from the Raman spectra of the trapped nanoparticles.

Authors noted that in the experiments the SWOT was formed by the interference between the incident beam and the reflected beam from a reflecting mirror such that the optimum trapping position was very close to the mirror surface. In the further improvement they wanted to use two counter-propagating tightly focused laser beams to form a stable standing-wave optical trap for 3-dimensional manipulation of nanoparticles.

4.6 EDU-OT2/M Portable Optical Tweezers [25].

This training set is optimized for use in classrooms and laboratories. The training set is assembled on a 30 cm x 60 cm (1 x 2 inch) aluminum optical plate.

The EDU-OT2 (/M) kit is equipped with a L658P040 laser diode with a wavelength of 658 nm as the trap laser source. This 40mW visible laser makes it easy to observe the laser spot through a microscope while working for visual demonstrations in the classroom. The laser is focused through a Zeiss 63X, NA 0.8 objective, which also serves as a microscope objective. The sample is illuminated with a white MCWHL5 LED and the sample is viewed with a Thorlabs DCC1645C color CMOS camera.

Samples are placed using a 3-axis positioner. The system consists of two motorized translators MT1-Z8 MT1 / M-Z8) with a travel range of 12 mm in the X and Y axes, as well as a mechanical translator MT1B (MT1B / M) for movement in the Z axis. Motorized translators are controlled by KDC101 servo controllers with adjustable speed.

5 Principles of optical spectrometer operation

5.1 Introduction

An optical spectrometer is an instrument used to measure properties of light over a specific portion of the electromagnetic spectrum, typically used in spectroscopic analysis to identify materials. The variable measured is most often the light's intensity but could also, for instance, be the polarization state. The independent variable is usually the wavelength of the light or a unit directly proportional to the photon energy, such as reciprocal centimeters.

5.2 Grating-based spectrometers

Spectrometers may operate over a wide range of non-optical wavelengths, from gamma rays and X-rays into the far infrared. The majority of spectrometers are used in spectral regions near the visible spectrum.

In general, any particular instrument will operate over a small portion of this total range because of the different techniques used to measure different portions of the spectrum. Below optical frequencies, the spectrum analyzer is a closely related electronic device.

Spectrometers are used in many fields. For example, they are used in astronomy to analyze the radiation from objects and deduce their chemical composition.

The general view of a spectrometer is shown in the Fig. 3.

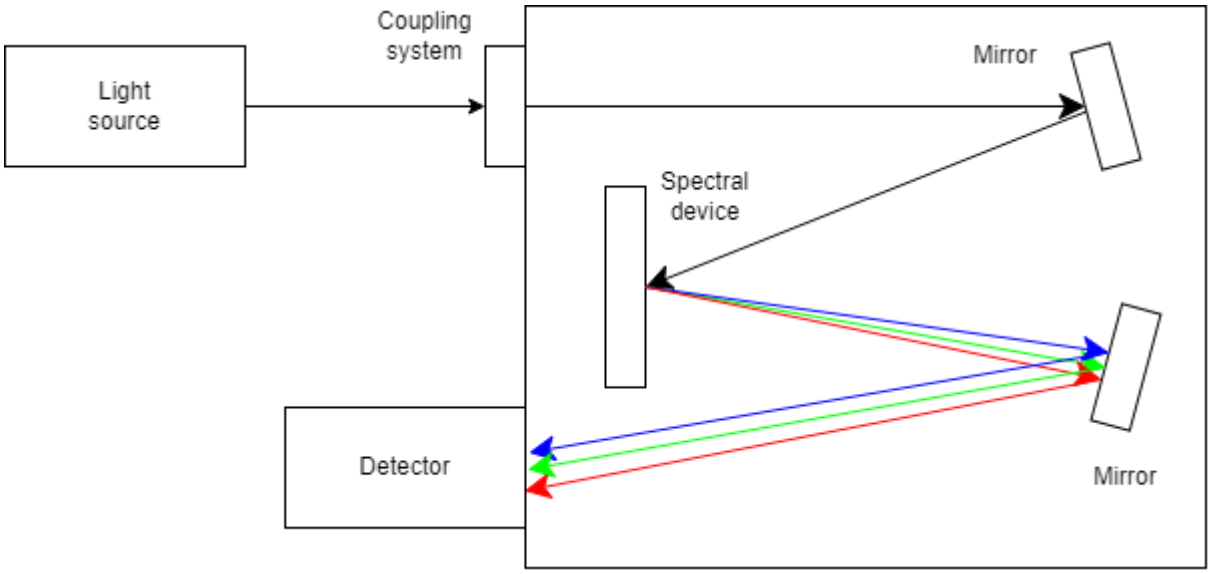

Fig. 3: General view of a spectrometer

At the first stage, the light enters the spectrometer through a narrow aperture, known as the entrance slit. In most spectrometers, the incident light is then collimated with a concave mirror and directed onto a spectral device (diffraction grating). The grating reflets the spectrum components at slightly different angles, which are then focused by a second concave mirror on a detector. The detector must be calibrated. The calibration is performed with special calibration lamps (Ne, HgAr) which emit a known spectrum.

5.3 Slit

The performance of the spectrometer depends on the entrance slit, since it determines the size of the light flux that enters the optical part. Spectral resolution depends on it, other important factors are the frequency of diffraction grating and the pixel size of the detector.

The optical resolution and throughput of the spectrometer depend on the slit parameters. The angle of divergence of the light entering inside depends on the slit.

The slit can have different widths - from 5 microns to 800 microns or more, the height of the slot is 1 mm (standard) - 2 mm.

Basically, slits 10, 25, 50, 100, 200 μm wide, etc. are used in spectrometers. In systems that use optical fibers to deliver the light beam, the size of the fiber bundle is the same as the size of the entrance slit. This usually reduces light scattering and increases the throughput of the instrument.

5.4 Diffraction grating

As we can see from the grating equation $dsin(\alpha_m) = m\lambda$, the main maxima depend on wavelength or there is an angular dispersion $d\alpha_m/d\lambda \neq 0$. The grating decomposes an incident non-monochromatic light into the spectrum. Thus, a diffraction grating is usually used as a spectral device in spectrometers. [17]

The simplest example of a diffraction grating is a slit grating, which is a set of a large number of identical parallel slits at equal distances from each other. It is this particular view of the diffraction grating that is shown in Fig. 4 but first we will carry out calculations for the general case of an array consisting of a set of N periodically located diffracting elements with a period *d*. Let us assume that the wave is incident normally to the grating plane.

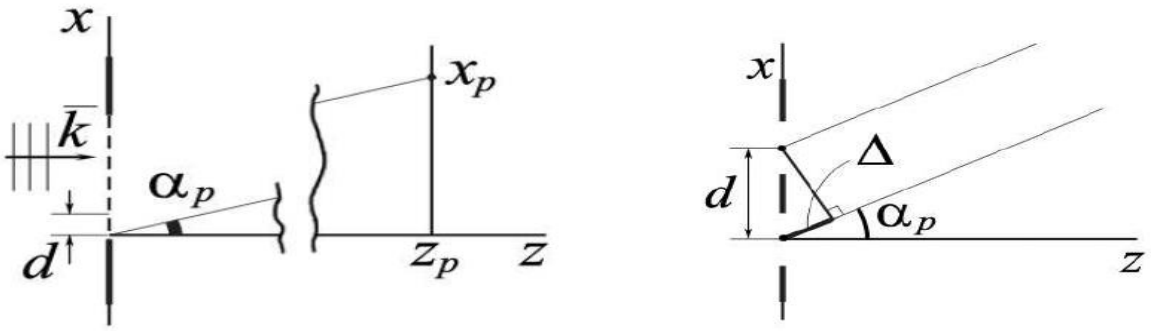

Fig. 4: Slit grating; x_p, z_p — observation plane coordinates, $\alpha_p = x_p/z_p$ — angular coordinate. $\vec{k}$ — incident wave. Δ — optical path difference.

Therefore, the electrical field in the observation point

$$\vec{E}(\alpha_p) = \overrightarrow{E_1}(\alpha_p)\left[1 + e^{-ik\Delta} + e^{-2ik\Delta} + \ldots + e^{-i(N-1)k\Delta}\right] \tag{13}$$

consists of N terms generated by a periodic structure (number of lines in a diffraction grating), and from each next element the wave comes with a phase shift due to the path difference $\Delta = \alpha_p d$ (Fig.4), where $\overrightarrow{E_1}(\alpha_p)$ is the field amplitude coming from a single element of the grating. The result of summing the obtained geometric progression gives the field at the observation point

$$\vec{E}(\alpha_p) = \overrightarrow{E_1}(\alpha_p) e^{-\frac{ik(N-1)\Delta}{2}} \frac{\sin\left(\frac{Nk\Delta}{2}\right)}{\sin\left(\frac{k\Delta}{2}\right)} \tag{14}$$

and the intensity

$$I(\alpha_p) = \left|\vec{E}(\alpha_p)\right|^2 = I_1(\alpha_p) \frac{\sin^2\left(\frac{Nk\Delta}{2}\right)}{\sin^2\left(\frac{k\Delta}{2}\right)} \tag{15}$$

In the specific case of a simple grating consisting of slits of width a, we have from [17]

$$I_1(\alpha_p) = I_0 sinc\left(\frac{ka\alpha_p}{2}\right) \tag{16}$$

Intensity $I(\alpha_p)$ is characterized by angle distribution schematically shown in Fig. 5

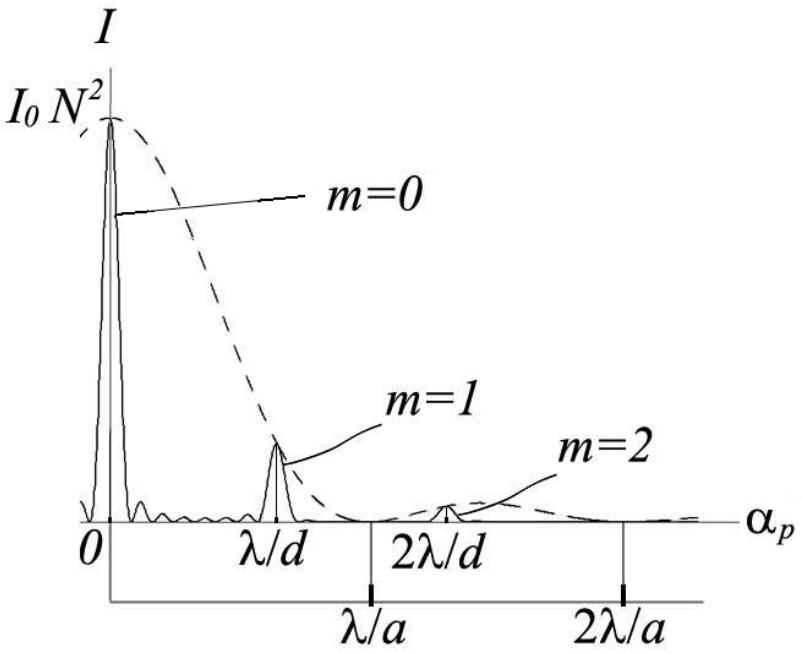

Fig. 5: Intensity distribution of slit grating. The dotted line corresponds to the function $I_1(\alpha_p)$.

Note that in the slit grating, only a small part of the incident light enters the diffraction maximum of some order $m \neq 0$. This is a serious shortcoming in the study of radiation from weak sources. It is eliminated in the so-called phase gratings, which make it possible to concentrate most of the energy of diffracting light in one or two main maxima. As an example, let us take a phase grating made of a transparent dielectric (for example, glass) with a groove profile shown in Fig. 6. The width of a line, which is also the period, is equal to d and $\beta << 1$. The amplitude of the field of the wave that passes through the grating is constant in absolute value. The phase in the $z = +0$ plane depends on the x coordinate, and its variable part is determined by the optical path length Δ, which consists of two parts. Within $0 < x < d$ of single line $\Delta(x) = nsin(\beta)x + (\sin(\beta)\, d - \sin(\beta)\, x) = n\beta x + (\beta d - \beta x)$, where the first term corresponds to a section of the path in glass with a refractive index n, the second to the layer of air (Fig. 6). Thus, without taking into account the constant phase factor $e^{(ik\beta d)}$, the intensity from single line is taken as

$$I_1(\alpha_p) = I_0 sinc^2\left[\frac{kd\left(\alpha_p - \beta(n-1)\right)}{2}\right] \tag{17}$$

This function differs from (16) only by argument of *sinc* function. But thanks to this difference, the central maximum of the $I_1(\alpha_p)$ function now occupies an adjustable position $\alpha_p = \beta(n-1)$.

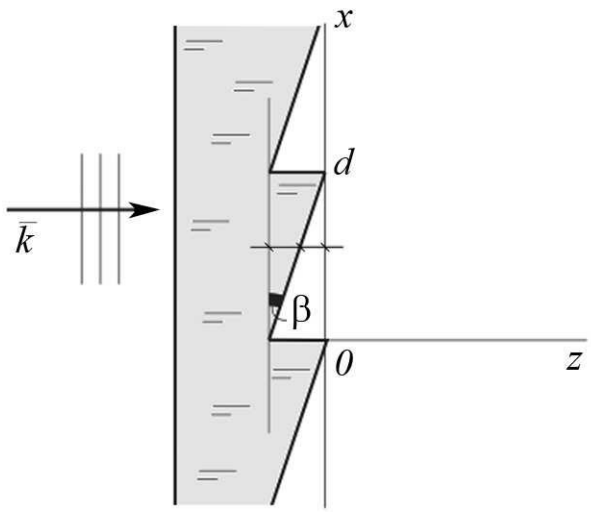

Fig. 6: Phase grating.

It is obvious that it is possible to achieve that the total intensity of the diffracted wave is characterized by just one main maximum by equating the value $\beta(n-1)$ to one of the maxima *mλ/d*; as shown in Fig. 7. Which corresponds to the case $\beta(n-1) = \lambda/d$. Here all the light incident on the grating is concentrated in one first maximum.

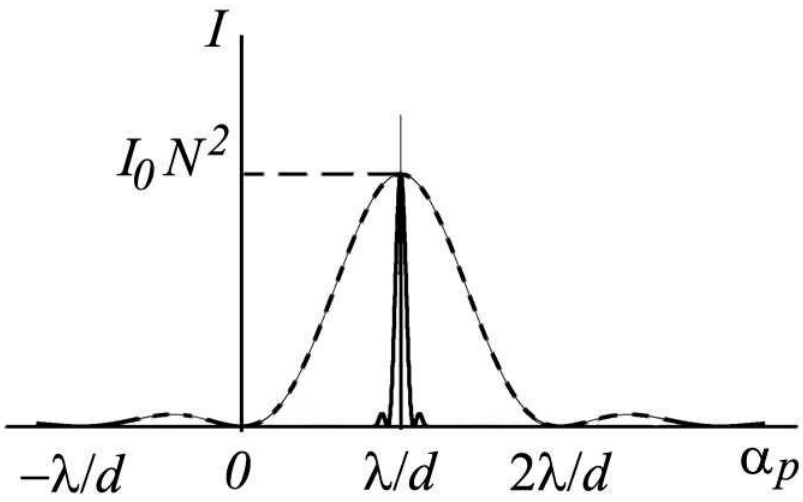

Fig. 7: Intensity of phase grating.

5.5 Resolution

Resolution of a spectral instrument $R = \lambda/\delta\lambda$ is defined as the ratio of the wavelength to the minimum wavelength difference that can be resolve by the instrument. The physical factor limiting the resolution of a diffraction grating is the finite angular width of the diffraction maximum. A fragment of the angular distribution of the intensity of the m-th maximum (normally m = 1 in practice for spectrometers) for wavelength λ is shown in Fig. 8. The width of this contour at half height, denoted ε, can be estimated as $\varepsilon \sim \lambda/Nd$.

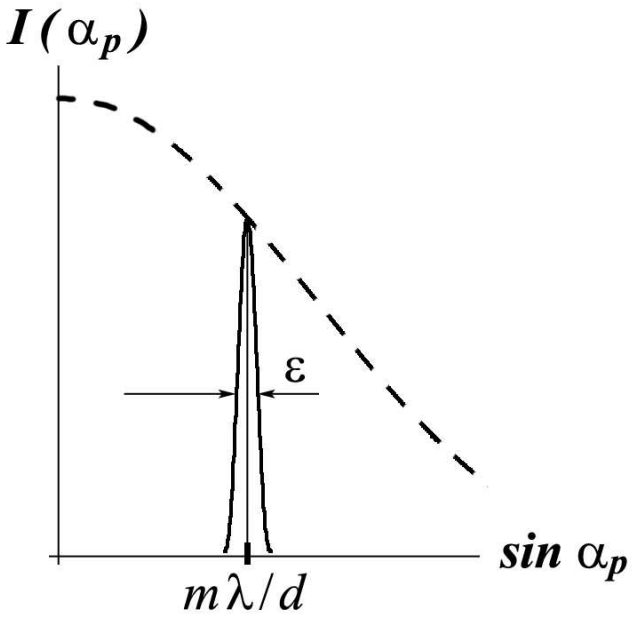

Fig. 8: FWHM of the m-th maximum.

If the contours of the maxima of the m-th order for the waves λ and $\lambda + \delta\lambda$ along the coordinate $\sin(\alpha_p)$ are moved apart by the value ε, as shown in Fig. 9, such lines are still resolved by a diffraction grating, since the total intensity contour shows a small dip in the middle. Since the centers of the maxima of the m-th order for the waves λ and $\lambda_1 = \lambda + \delta\lambda$, $\lambda_2 = \lambda - \delta\lambda$ are determined from the grating equation $dsin(\alpha_m) = m\lambda$, for the difference $sin(\alpha_m{}^{(1)}) - sin(\alpha_m{}^{(2)})$ we obtain the value $m(\lambda_1 - \lambda_2) = m\delta\lambda/d$. For resolvable lines, this value should be equal to ε, i.e. $\frac{m\delta\lambda}{d} = \frac{\lambda}{Nd}$ and $R = Nm$.

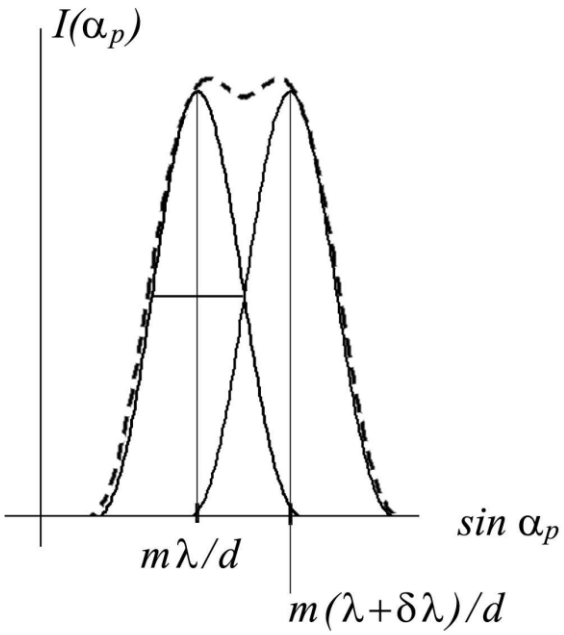

Fig. 9: Diffraction grating resolution.

Thus, the resolution *R* of the diffraction grating is proportional to the number of lines N in the grating.

At the same time, the resolution of the entire spectrometer is determined by three key parts of the device: the entrance slit, the diffraction grating, and the detector. The slit determines the minimum image size that the optical system can form in the detector plane. The diffraction grating determines resolution and spectral range. The detector determines the maximum number and size of pixels that can be digitized as a spectrum.

6 Experimental setup and equipment

6.1 Setup

In this work a home-built upright Raman microscope setup was used. The main principle was to use the same strong laser radiation for both optical trapping of tested particles and excitation of Raman scattering. The optical setup scheme is presented in Fig. 10.

The continuous-wave diode pumped laser **1** [18] (DPL) operating at a fixed wavelength of 660nm was used. The power was 500 mW and beam diameter at the aperture was 700 ±50 μm. The expander consisted of two lenses **4** (Thorlabs LC4252-A) – a plano concave lens with focal length -30 mm and **5** (Thorlabs LA4158-A-ML) – a plano convex lens with focal length 250 mm. It expanded the laser beam by the factor of 8.3 so the beam fitted the aperture of the objective 10. The beam was filtered with a narrow band pass filter **6** to get rid of parasite wavelengths. Then the beam was transferred from the horizontal to the vertical plane by a dichroic mirror **7** (Semrock Di03-R660-t1-25x36) and a system of three mirrors **8**. The laser beam was focused by a water-immersion infinity corrected objective **10** OLIMPUS UPLSAPO60XW [19] with working distance 0.28 mm and numerical aperture 1.2. Sample holder **11** consisted of two borosilicate cover slips and later two quartz cover slips. A solution of diluted in water polystyrene beads with volume of 5-10 μm^3 was sandwiched between the two cover slips. The same objective was used to collect the Raman signal, deliver it thought the coupling system **18**, **19** to the spectrometer **21** (IsoPlane 320A [20]). At the same time the objective was used to image the sample (sector **c**, parts 12-17).

At first, the laser's sector **a** was aligned and collimated using principles of linear optics. Position and angle of the laser beam were controlled by mirrors **2** and **3**. A collimated beam was achieved by beam expander lenses **4** and **5**. The beam was filtered with the filter **6**.

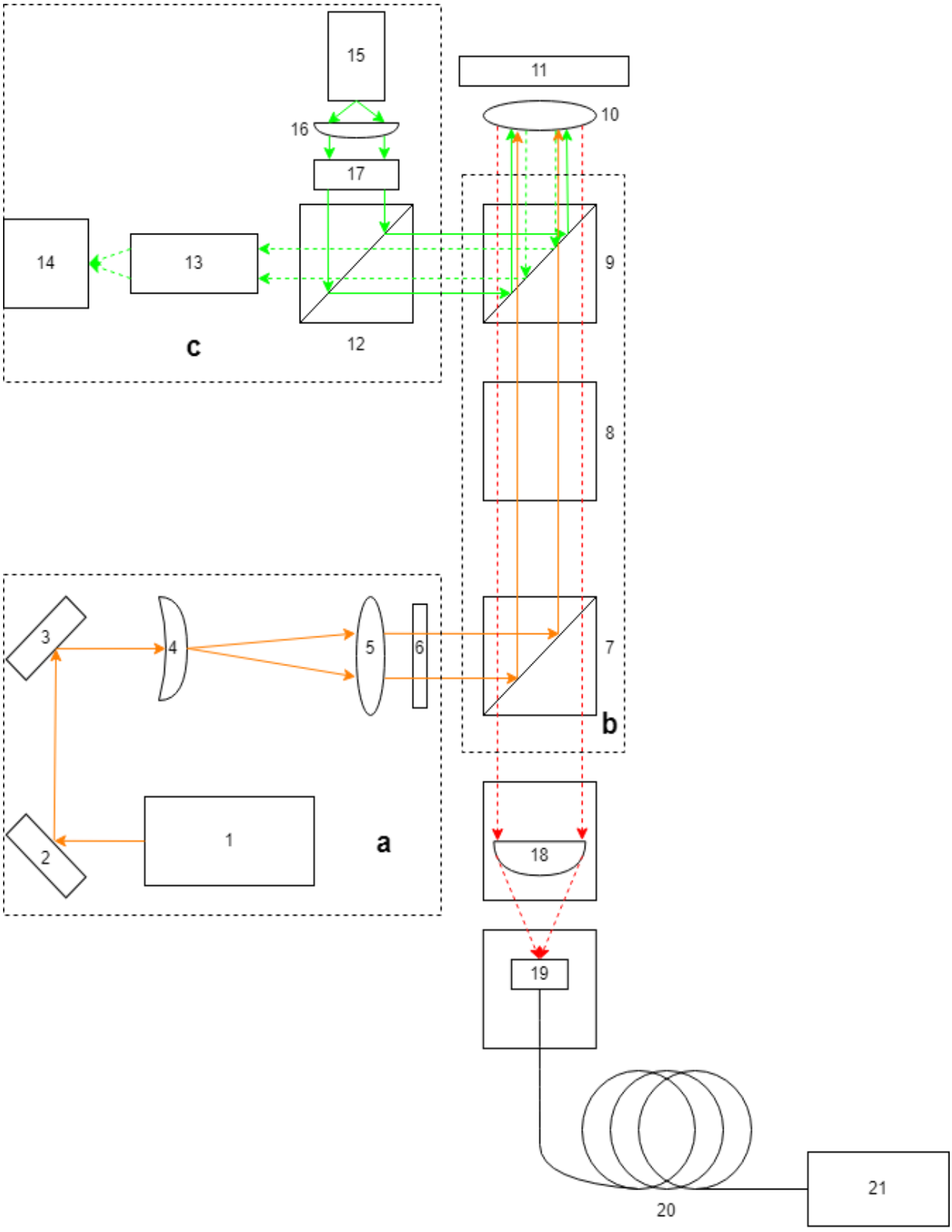

Fig. 10: The setup. ***1*** *– laser;* ***2,3*** *– mirrors;* ***4,5*** *– beam expander lenses;* ***6*** *– band pass filter;* ***7*** *– 635nm dichroic mirror;* ***8*** *– mirror system;* ***9*** *– dichroic mirror;* ***10*** *– water immersion 60x objective;* ***11*** *– sample;* ***12*** *– 90/10 split mirror;* ***13*** *– tube lens;* ***14*** *– CCD;* ***15*** *– 535nm LED;* ***16*** *– LED lens;* ***17*** *– iris;* ***18*** *– 10x objective;* ***19*** *– fiber coupling;* ***20*** *– multimode fiber;* ***21*** *– spectrometer;* ***a*** *– laser sector;* ***b*** *– microspoce sector;* ***c*** *– imaging system.*

Further, the objective sector **b** was configured. A dichroic mirror **7** was fixed on a kinematic cage cube in such a way that it was possible to control the direction of the beam. Mirror system **8** was used for alignment of the beam in this sector. Therefore, the expanded and aligned laser beam hit the objective from above. Dichroic mirror **9** in this sector was used as transmission element.

6.2 Imaging System

Next, the imaging system **c** was set up. LED **15** (Thorlabs M656L3) with nominal wavelength 565 nm was used as a light source. The light was collimated by the lens **16** (Thorlabs ACL2520U). Then it was split by the beam splitter **12** (Thorlabs CM1-BP108) and directed to the objective **10** by the dichroic mirror **9** (Di03-R635-t3-25x36). 635 nm.

Objective **10** collected reflected light from sample **11**. Dichroic mirror **9** directed it into the tube lens **13** (OLYMPUS SWTLU-C focal distance – 180 mm) which focused the beam onto the CCD camera **14** (iDS uEye UI-1240SE-M-GL).

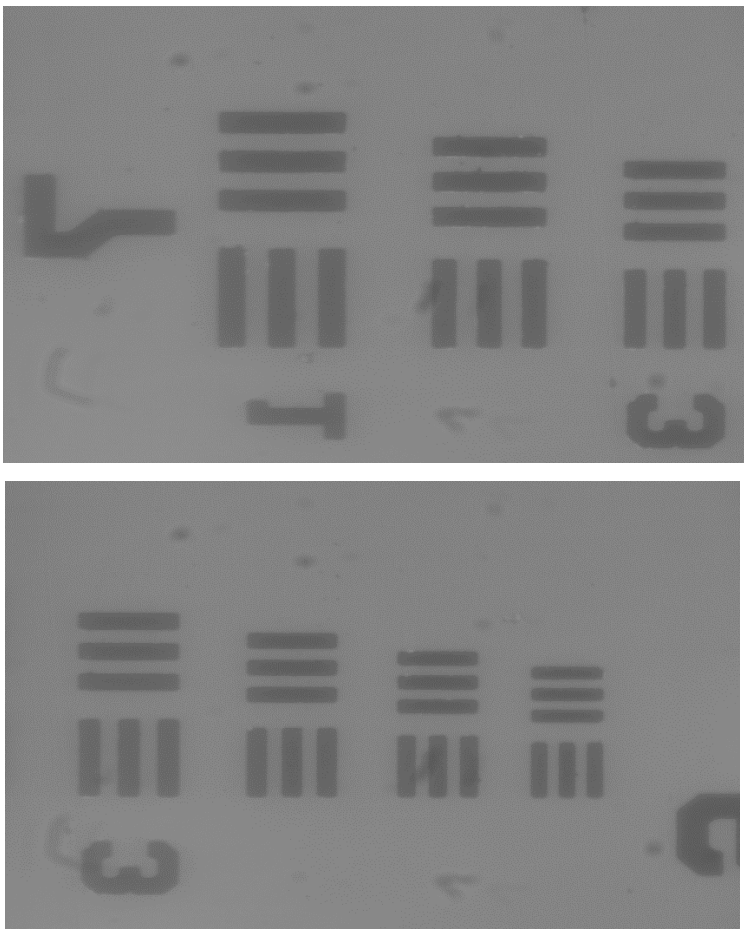

Fig. 11: Images of the resolution target USAF 1951 group 7 elements 1-6 obtained with the home-build microscope.

Further, the test images of the resolution target USAF 1951 [21] (Fig. 11) were obtained with different objective (Olympus MPlanFL N 50x). They were compared to the images of the same resolution target (Fig. 12) obtained with the commercial microscope available in the university.

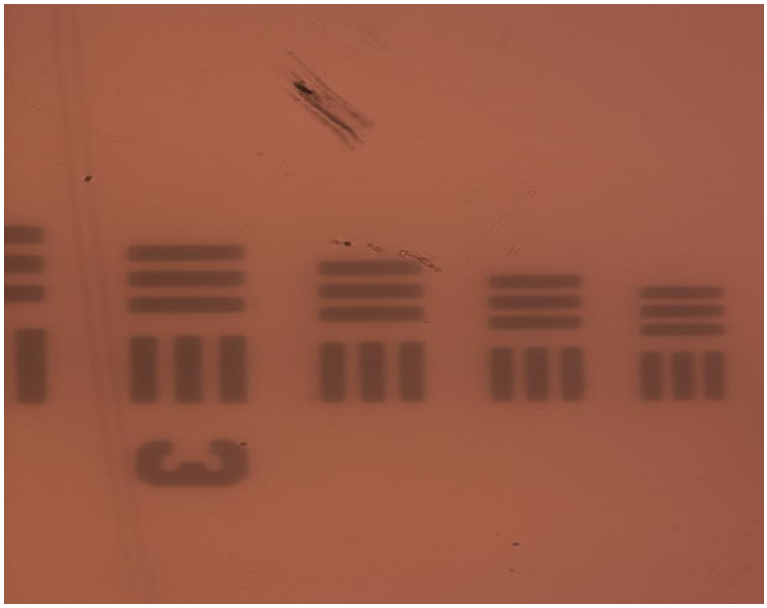

Fig. 12: Image of the resolution target USAF 1951 group 7 elements 1-6 obtained with the commercial microscope.

As we can see from the figures, the images obtained with the microscopes are almost the same. It was possible to resolve clearly the smallest element in the smallest group in this target. Where the width of a line is 2.19 µm. The resolution is 228.1 lm/mm according to [21].

Further, the optical paths of the reflected signal (red dotted line in Fig. 8) and the laser (orange line) were aligned.

For this, the spectrometer **21** was replaced by a laser (Thorlabs LP685-SF15) with a wavelength of 685 nm to imitate the signal reflected from the sample. It was made so that both optical paths occupied the same position and had the same angle in section **b**, using all the optical components in sections **a** and **b**. Also, an additional criterion was the identical positioning of the beams of two lasers on the CCD camera **14** (Fig. 13). To do this, the camera acquisition time and the power of laser 1 were set to the minimum.

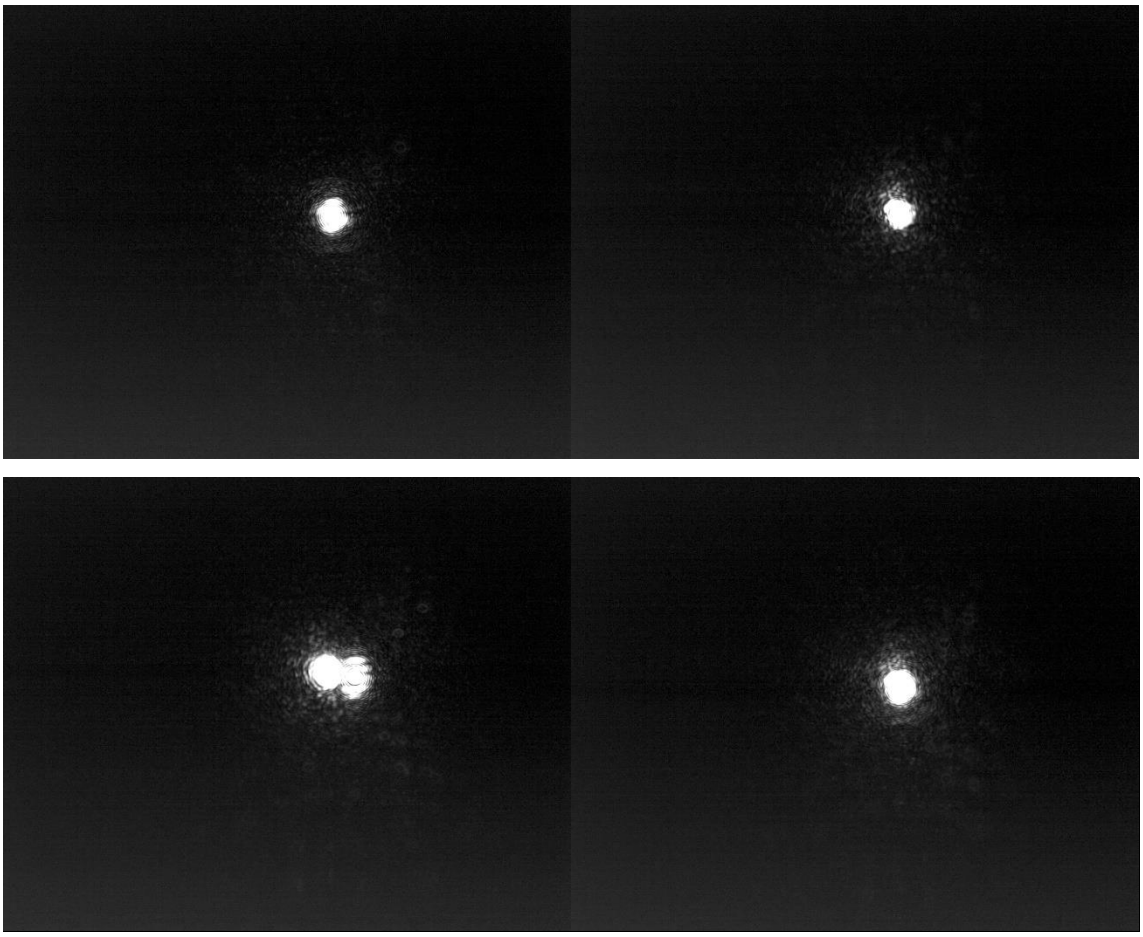

Fig. 13: The beams positioning on the camera. Left-upper corner – spot from the 660 nm laser. Right-upper corner – spot from the 686 nm laser. Left-lower corner – two misaligned spots. Right-lower corner – two aligned spots.

As one can see from the Fig. 13, the spots of the two lasers were good aligned and this condition was used to check the alignment before the experiments.

Farther, the images of the polystyrene beads with the diameter of 7 μm were obtained (Fig. 14)

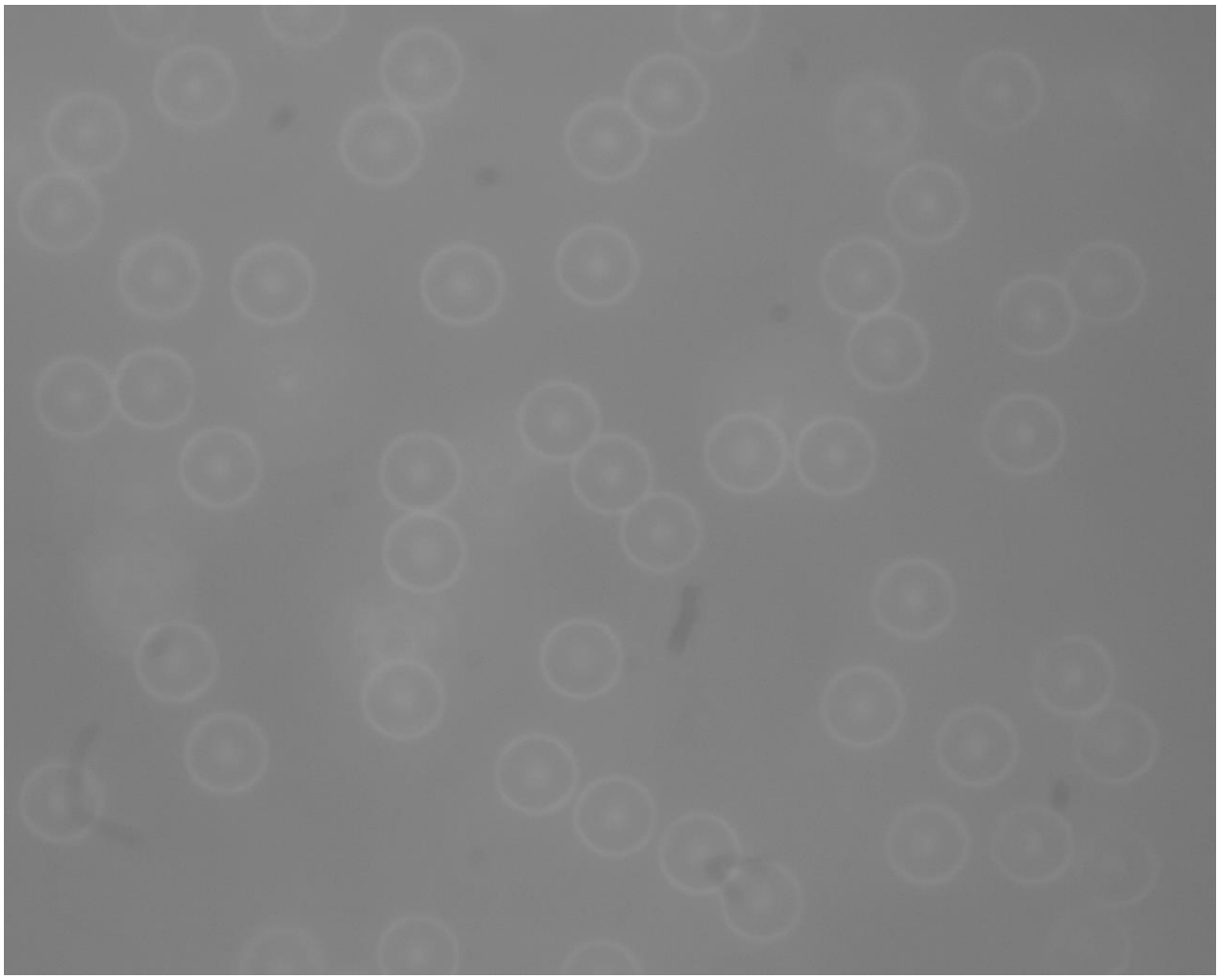

Fig. 14: Image of 7 µm polystyrene (PS) beads.

6.3 Optical Trapping

The next step was to trap particles in the setup (Fig. 15). To do this, 7 µm PS beads, 20x objective were used. The laser beam power was set to 80 mW.

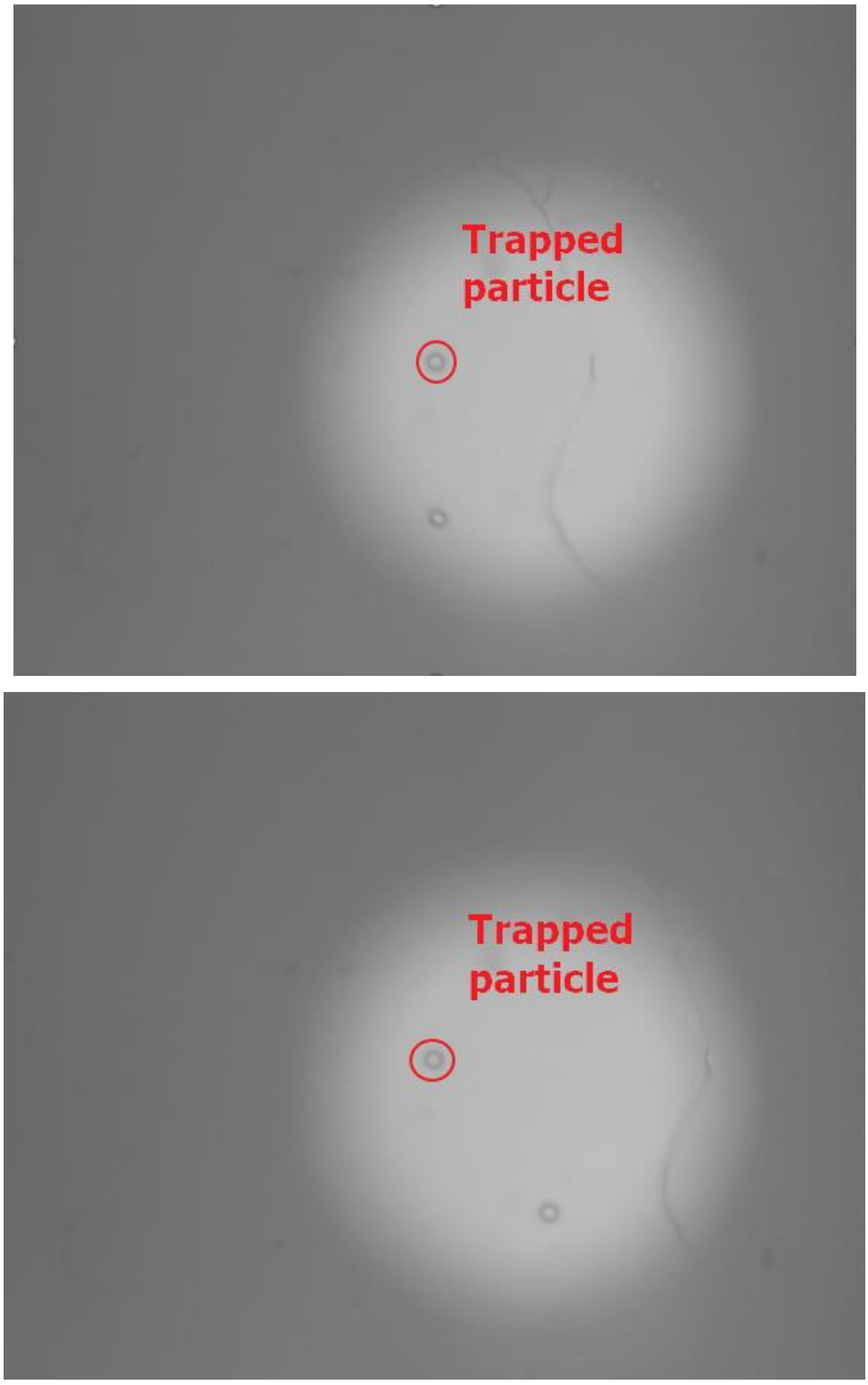

Fig. 15: Trapped 7 µm PS bead

As can be seen from Fig. 13, the particle was trapped and moved relative to other features of the sample. The stability of the trap was also checked. The particle was trapped for more than 10 minutes.

6.4 Diffraction grating

It was necessary to choose which diffraction grating to use. To do this, spectra were collected from a borosilicate cover slip at a laser power of 150 mW for three different diffraction gratings (Fig. 16).

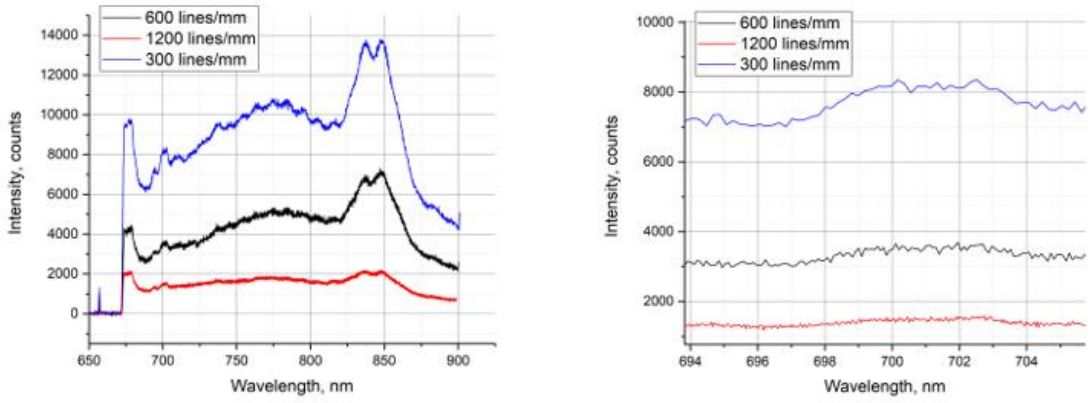

Fig. 16: Spectra from the different types of diffraction gratings. right – full span, left – zoomed in.

As one can see from the Fig. 16, the spectra differ in intensity and resolution as expected. The grating with 1200 lines/mm is the densest grating but has the lowest intensity response and vice versa the 300 lines/mm grating has the best intensity response but is the sparsest grating. Therefore, it was decided to choose the 600 lines/mm grating. Thus all data were collected on the grating of 600 lines/mm with a central wavelength of 720 nm and, accordingly, wavelength span from 650 to 780 nm.

6.5 Spectrum background

During the experiments, it was found that the background strongly dominates the useful signal. in fact, the first spectra from particles contained nothing but the background. Presumably, this was due to the fact that the trap was not optimized enough. The particles were pushed by the laser to the lower coverslip. Thus, preventing them from being kept at a sufficient distance from the glass in the solution. Where the contribution to the background would be predominantly from water. But since the particles were pressed against the glass, a lot of the light reflected from the glass hit the objective, making a big contribution to the background. An attempt was also made to deal with the background by replacing borosilicate glass with quartz glass, but this did not give noticeable results.

Several methods of background correction have been considered. At first, data were taken from only one coverslip. Next were two glasses. Then two cover slips and distilled water between them. In this case, the laser was focused into two different positions - approximately in the middle on the water between the glasses and as close as possible to the bottom glass, and, accordingly, the reflected light was collected from the same positions. The results are presented of the Fig. 17.

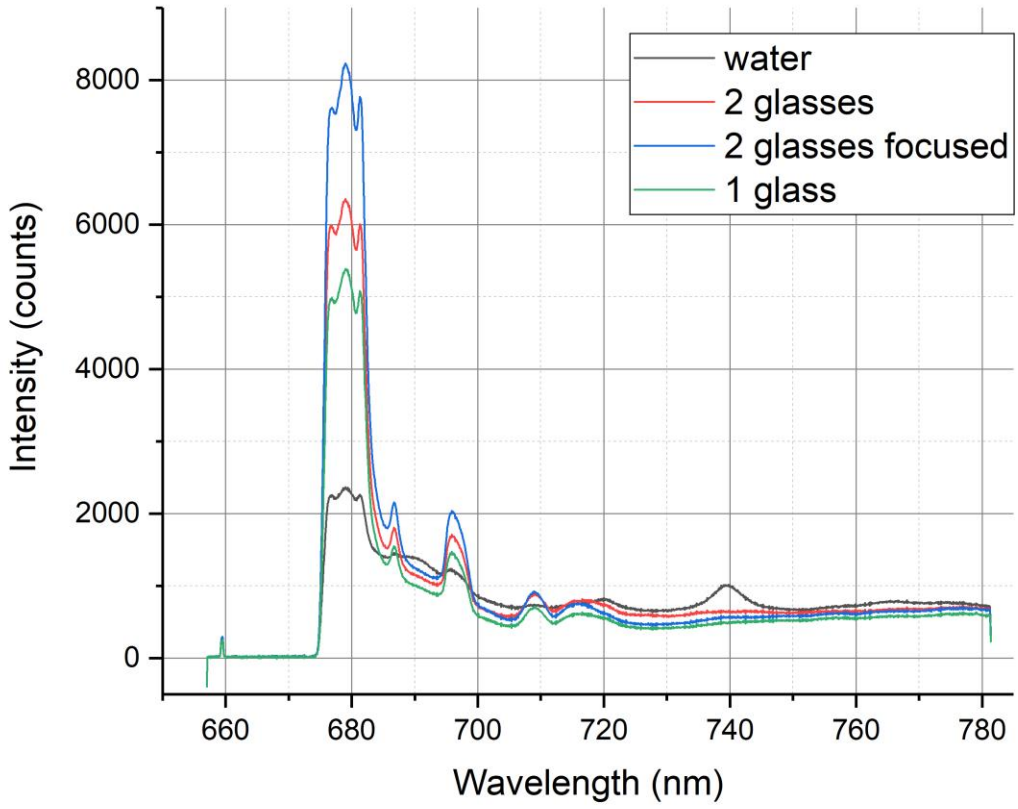

Fig. 17: The background from different sources.

It can be seen that the glass backgrounds do not qualitatively differ from each other, but they strongly depend on how the laser was focused and it changes from experiment to experiment. The water background at the same time was low and more uniform in terms of focus point. Thus, it was assumed that the particle would be trapped in the middle of the solution and, accordingly, the contribution to the background would be only from water. but as mentioned above, this was not achieved and particles were often pressed against the glass. Therefore, when correcting the background, the data obtained from the glass were taken into account.

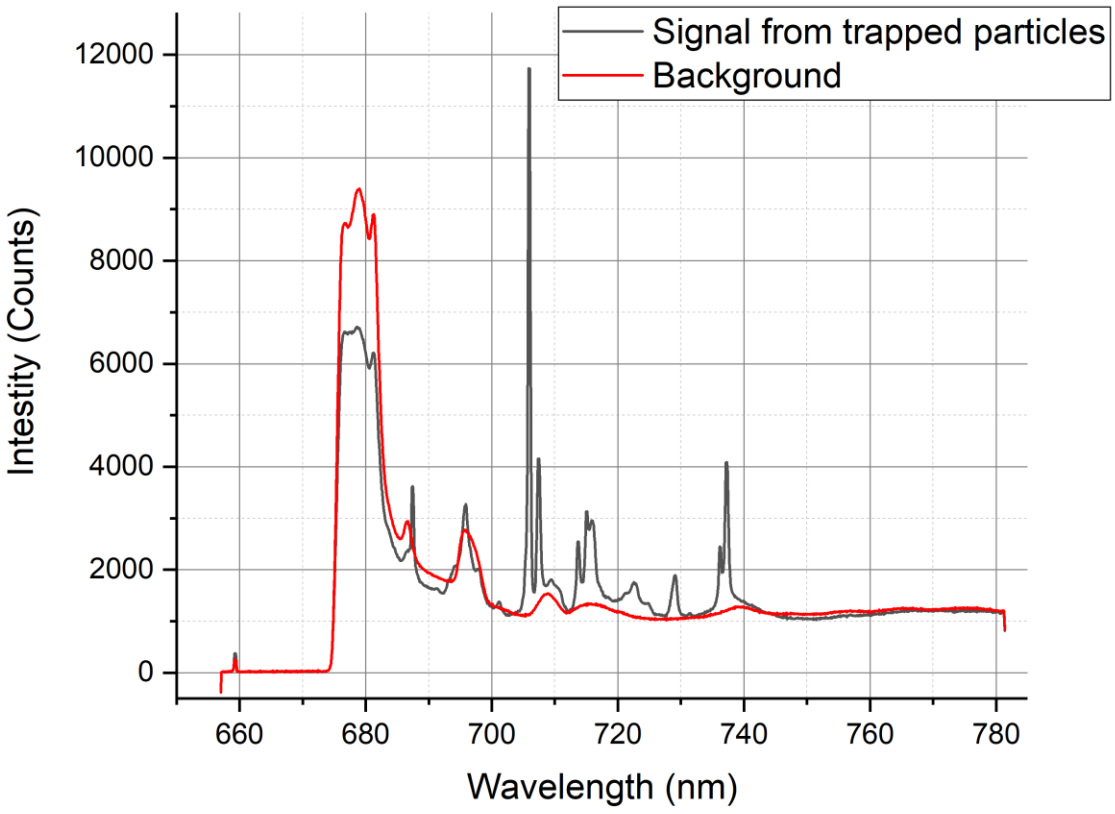

Fig. 18: Background analyzation.

The following is an example of how the background was actually corrected. In fig. 18 it can be seen that the Raman signal from the particles is well distinguishable, but the spurious background is rather high. To correct it, a signal was taken from the glass right before the experiment (red line). It was assumed that the background can be simply subtracted from the signal or make a linear fit of the background: $S(\tilde{\nu}) = B + f(\tilde{\nu})$, where $S(\tilde{\nu})$ is general signal, B – background and $f(\tilde{\nu})$ – Raman scattering, $\tilde{\nu}$ – Raman shift.

But the figure clearly shows that the background depends on the wavelength. Accordingly, it was proposed to introduce a certain weight function to fit the background to the signal. $S(\tilde{\nu}) = B \cdot \omega(\tilde{\nu}) + f(\tilde{\nu})$, where $\omega(\tilde{\nu})$ – the weight function. It is easy to understand from the graphs that the function must be a logarithmic function or inverse hyperbola with an asymptote equal to 1. A hyperbola of the form $\omega(\tilde{\nu}) = 1 - \frac{1}{A \cdot \tilde{\nu}}$ was chosen, where A is the fitting factor which can be easily calculated from the data.

The result of the correction is shown in Fig. 19.

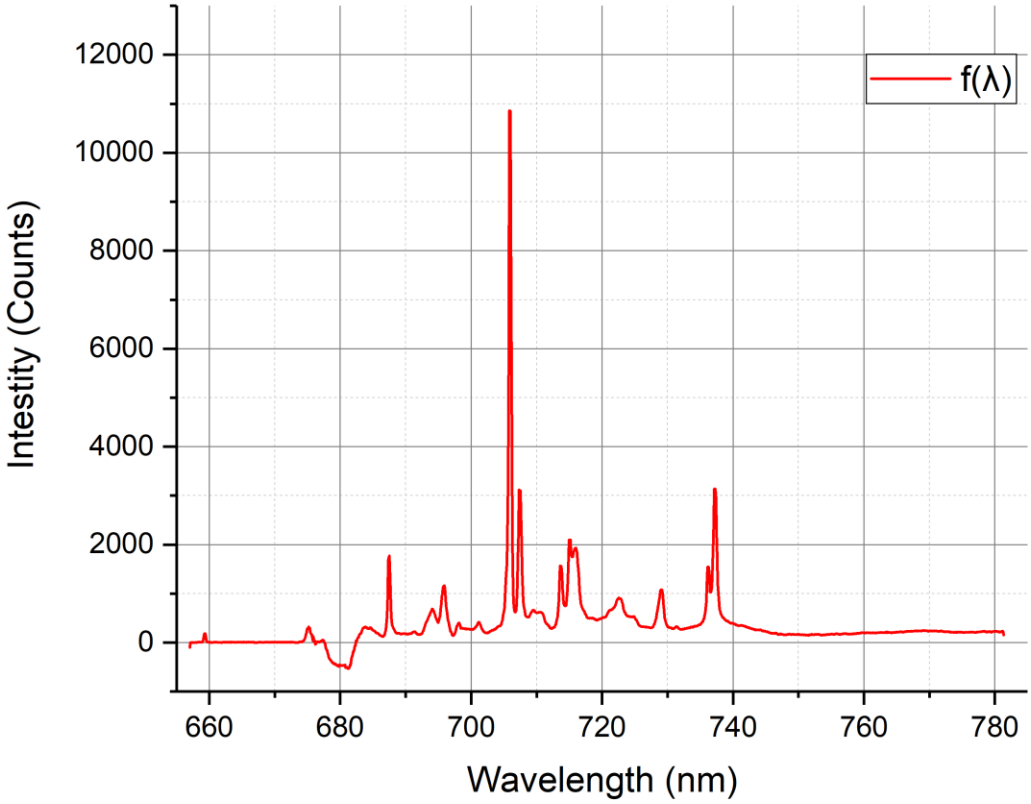

Fig. 19: Background correction.

7 Raman spectroscopy. Results and discussions

7.1 Introduction

After all the preliminary work was completed, acquisition of PS beads spectra began. Experiments were carried out with six particles of different sizes - 7, 5, 2, 1, 0.5, 0.2 microns. The results differ greatly for large (7 and 5 microns) and small (other) particles. Where for large particles the Raman signal was very weak, and the signal from small particles strongly depended on how many particles were in the trap. Usually there were few particles in the trap – approximately 1-5. Whereas small particles could easily reach dozens. Also, the signals were very susceptible to background from cover slips.

All the data presented were filtered with the in-build spectrometer software median filter to get rid of the cosmic rays. Also, to reduce the noise level, all spectra are presented as averages of several spectra.

7.2 Spectra of 7 and 5 μm polystyrene beads

The first experiments were done for 7 μm particles on the borosilicate cover slip. The procedure was as follow: in a diluted solution of microspheres in water the laser of power 100 mW was used to trap a single particle and excite the Raman scattering. The laser was focused with 50x and 0.8 NA objective. Scattered light was collected form the trapped particle with the same objective and sent to the spectrometer through the multimode fiber. Acquisition time of the spectrometer was 1 second. At first it was not possible to obtain any results, except for the background from the coverslip (Fig 20). Further, in order to check whether the correct signal is obtained, the laser was focused on tape of hole reinforcements which were used to localize the sample on the cover slip (Fig. 21).

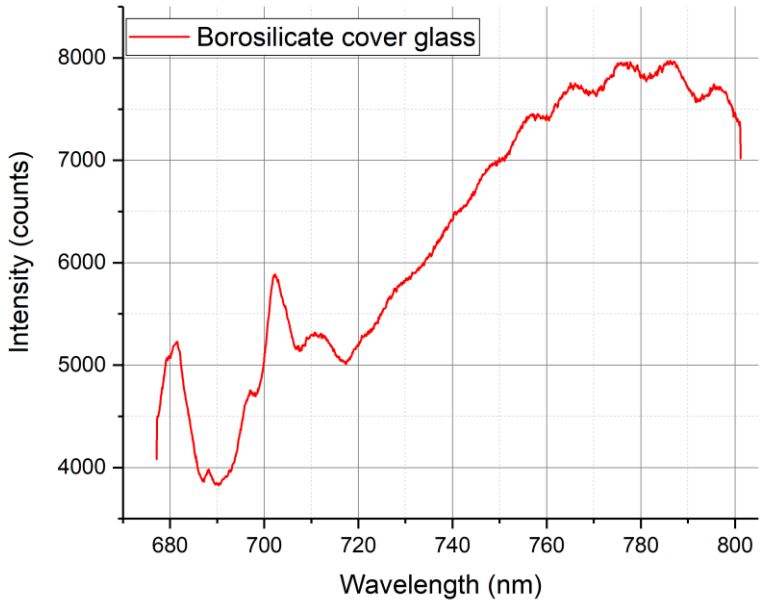

Fig. 20: Background spectrum from the borosilicate coverslip.

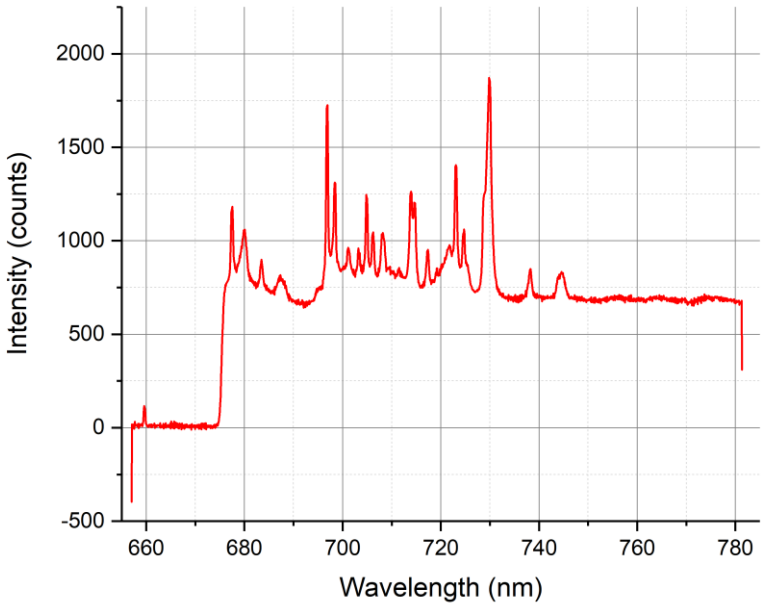

Fig. 21: Hole reinforcements tape.

After optimization of the laser focusing and background correction the 7 µm spectra were obtain. The spectrum is shown on Fig. 22.

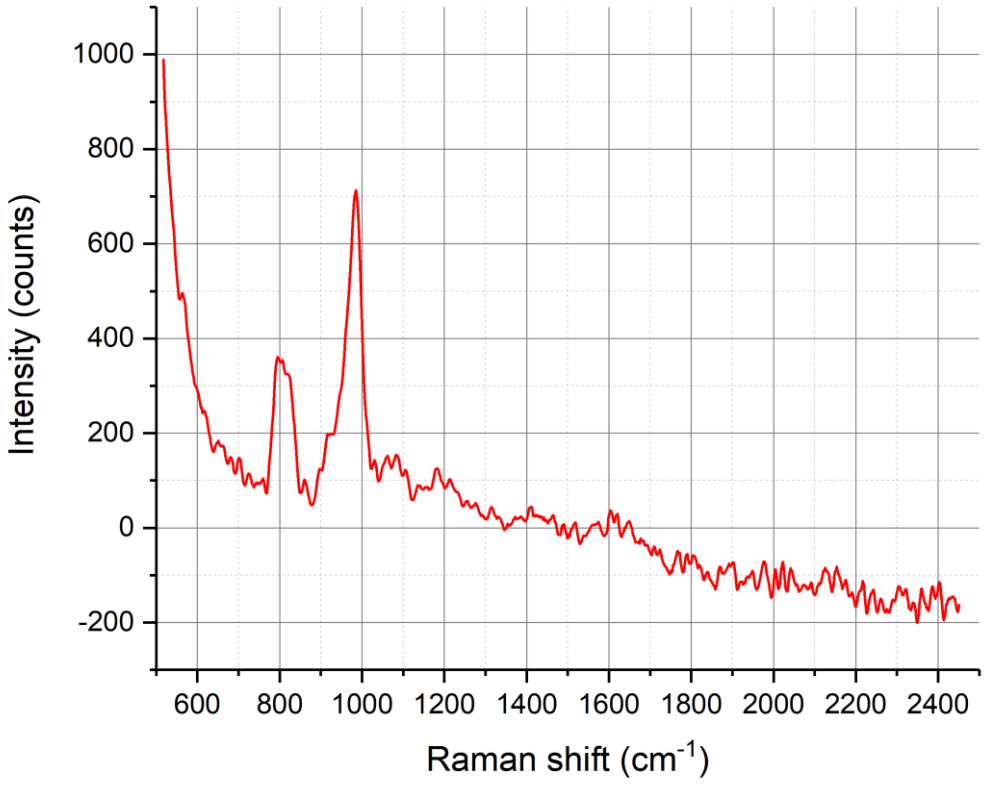

Fig. 22: Spectra of 7 µm PS bead, 1 second acquisition, average over 10 spectra.

There are 2 peaks on the graph, which most likely correspond to 1001.4 cm^{-1} and 795.8 cm^{-1} [22] with a small shift. An increase in the intensity of the spectrum beyond 600 cm^{-1} and below most likely corresponds to the Rayleigh radiation, which could not be eliminated at the stage of background processing.

Spectra were also taken for particles with a diameter of 5 µm. Quartz was now used as a cover slip. In addition, another procedure was performed: the top coverslip was removed and the specimen was allowed to dry. Thus, the particles adhered to the substrate and occupied fixed positions. thus they were easier to analyze and collect the spectrum. It also gave freedom in collecting the background. But in this case, the particles were not trapped, which in some way reduced the stability. The results are presented on Fig. 23.

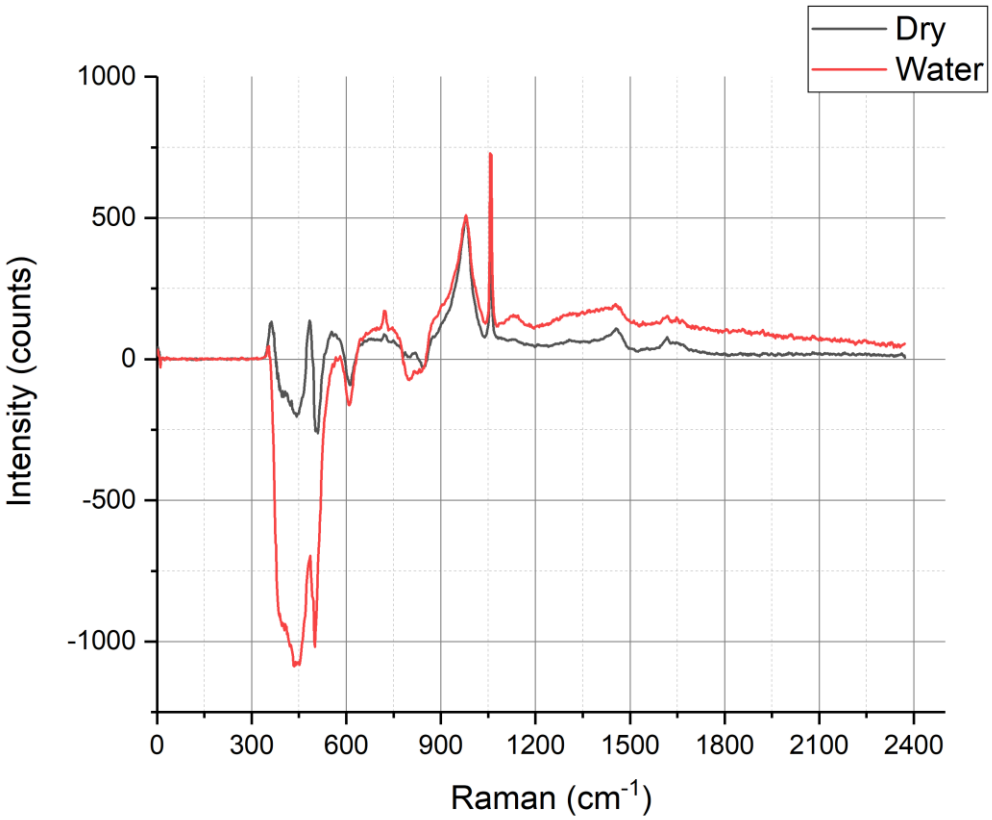

Fig. 23: Spectra of 5 µm PS bead, 1 second acquisition, average over 60 spectra.

The peaks at 1001.4 cm-1 and 795.8 cm-1 can also be easily distinguished in this figure. In addition, one can see the appearance of two peaks that possibly correspond to 1450.5 cm-1 and 1602.3 cm-1 [22]. As one can see, it was not possible to fully correct the background.

7.3 Spectra of 2, 1 and 0.53 µm polystyrene beads

After not the most successful attempts to take spectra from large particles (7 and 5 microns), it was decided to switch to smaller ones. The procedure of the experiments was as follows: The laser of power 500 mW was used to trap a cluster of microspheres (Fig. 24). The laser beam was focused by the 50X 0.8 NA objective and 60X 1.2 NA water immersion objective. Quartz glass was used as a substrate for the sample. For the trapping it was necessary to fish for the particles and optimize the focus by pressing them to the substrate.

The spectra for 2 µm particles are presented on the Fig.25 and 26.

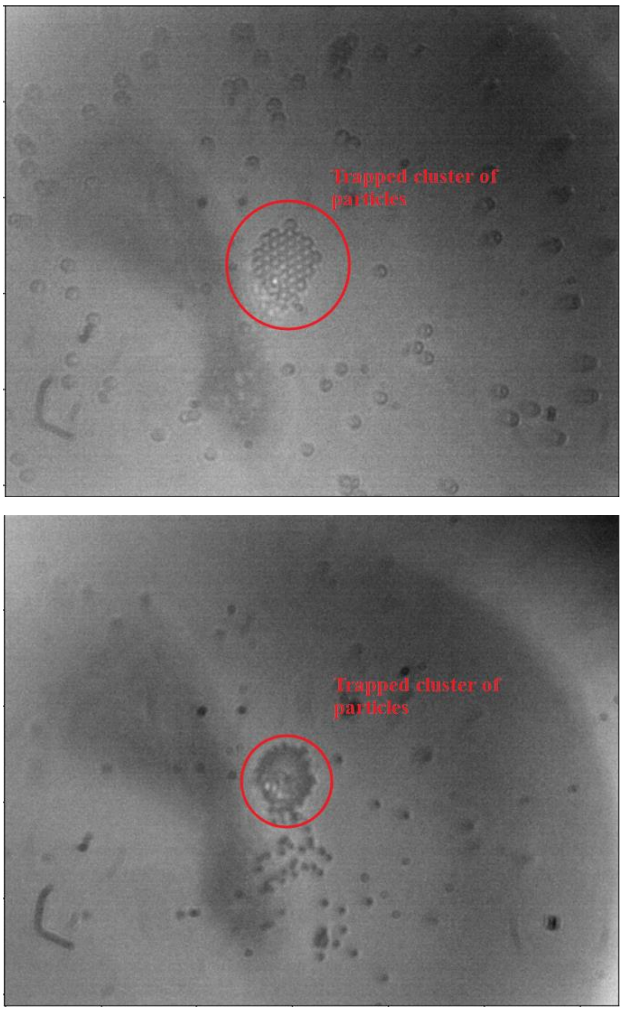

Fig. 24: Cluster of trapped 2 (right) and 1 (left) µm PS beads. Images of smaller particles (0.53 and 0.19 µm) could not be obtained.

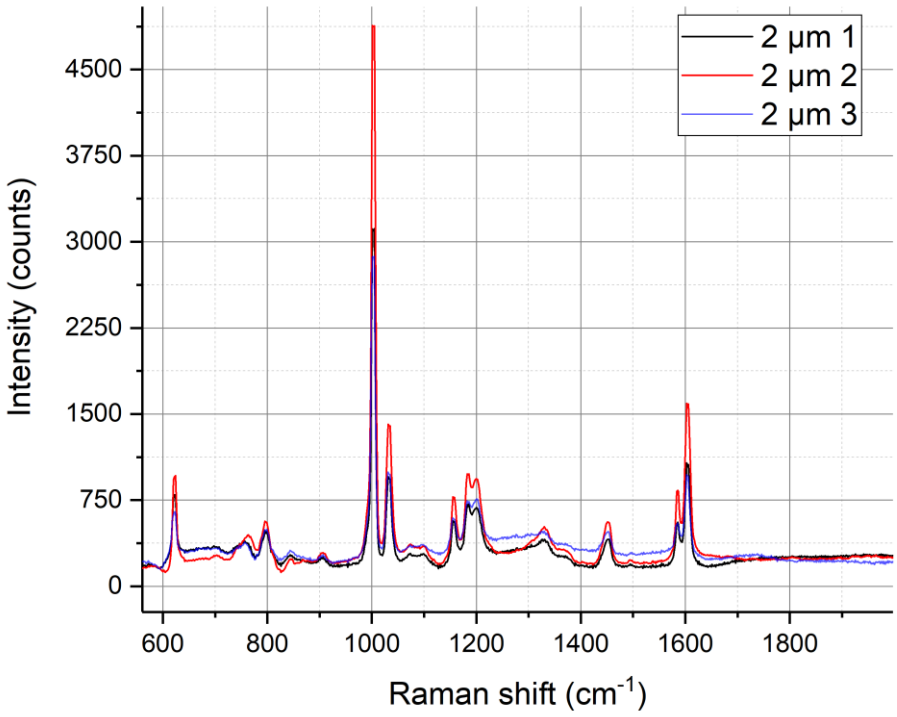

Fig. 25: 3 different sets of spectra of 2 µm PS beads. 1 second acquisition time. Average of 60 spectra. 50X 0.8 NA objective.

As can be seen from the graph, all the main peaks of the Raman spectrum are clearly distinguishable (Table 1).

Polystyrene peaks, cm^{-1}	Assignment
621	Benzene ring deformation mode
795	C-H out-of-plane deformation
1001	Benzene ring breathing mode
1031	C-H in-plane deformation
1155	C-C stretch
1450	CH_2 scissoring
1583	Benzene ring-skeletal stretch

Table 1: Main peaks of polystyrene Raman spectrum [22].

All three graphs differ in intensity. It strongly depended on focusing and the number of particles in the trap. If the focus dependence could be regulated, then the number of particles in the trap could not be controlled. It depended on the concentration of particles in the solution and on the thermal motion, due to which there was a constant flow of particles entering and leaving the potential well of the beam.

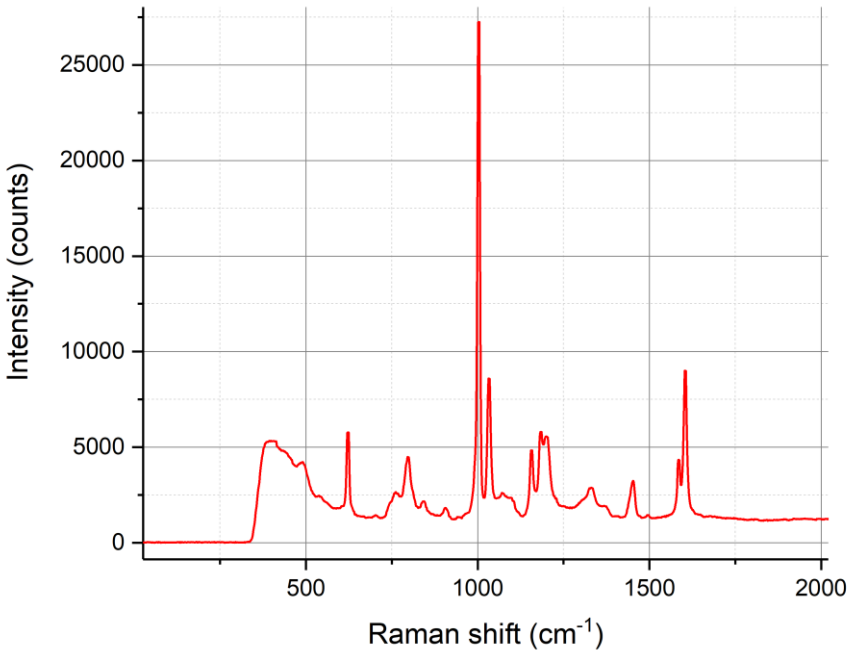

Fig. 26: Spectrum of 2 µm PS beads collected by 60x 1.2 NA objective. Average of 60 spectra.

As seen from Fig. 26, the spectrum for the 60x 1.2 NA objective has all the main polystyrene peaks. The intensity is an order of magnitude higher than for a 50x 0.8 NA objective. Despite the fact that the proportionality of peak intensities remained approximately at the same level. Due to the high intensities of the peaks, the background correction was not needed for this spectrum.

The spectra obtained for 1 µm particles are shown on Fig. 27.

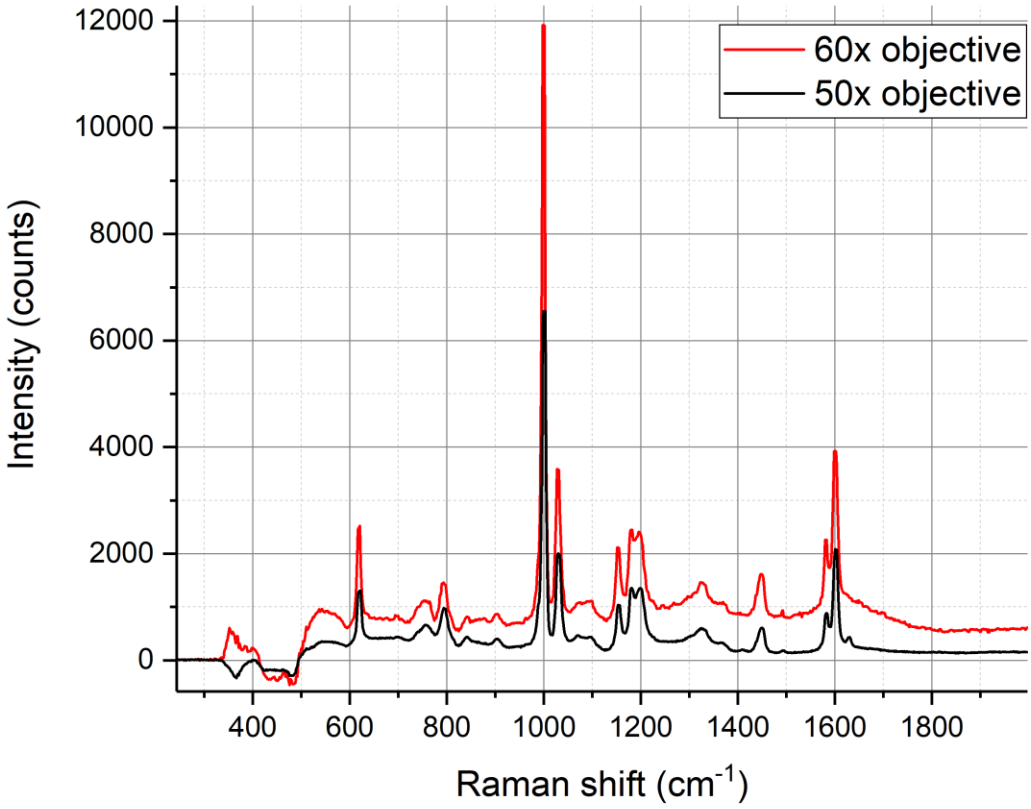

Fig. 27: Raman spectra of 1 µm particles acquired with 60x 1.2 NA and 50x 0.8 NA objective. Average of 60 spectra.

As expected, the intensity for a 60x lens is higher. all the main peaks are also visible for both objectives. The intensity for the 50x objective became slightly higher than for 2 µm particles. The intensity for the 60x objective doubled. But as mentioned above it strongly depends on where the focus was and how many particles were trapped.

Only 50x objective was used for 0.5 µm particles. Spectrum is presented on Fig. 28. Strong drop in signal intensity can be observed. But despite this, all the peaks are clearly distinguishable.

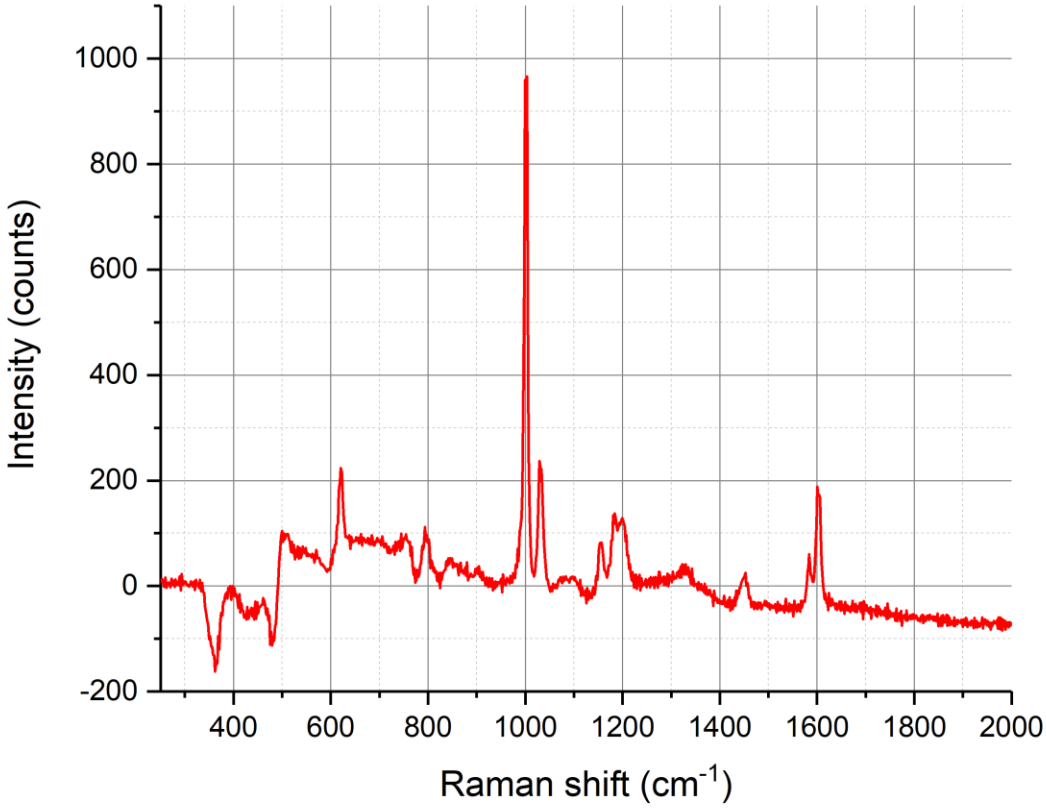

Fig. 28: Raman spectra of 1 µm. Average of 60 spectra.

7.4 Spectra of 200 nm polystyrene beads

The spectra of 200 nm polystyrene beads were obtained using laser of 500 mW, 50x 0.8 NA and 60x 1.2 NA objectives. The results are presented on Fig. 29.

a large decrease in intensity is observed for a 50x lens compared to a 60x one. But all the peaks can still be distinguished.

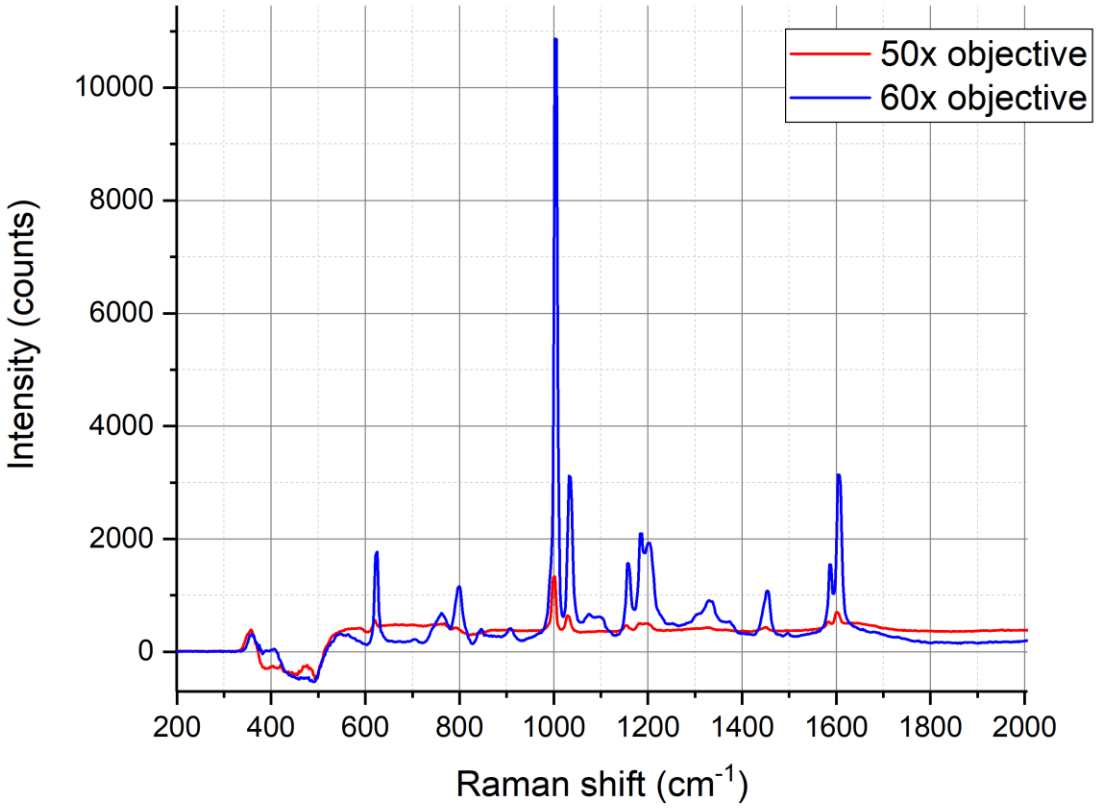

Fig. 29: Spectra of 200 nm PS beads. Average of 60 spectra.

A dynamic analysis of the spectrum was also carried out for the dependence on the in- and out-flow of particles from the trap. For this, a highly dissolved solution was taken. So that the initial number of particles in the trap is as small as possible. Then a certain number of spectra were taken in a row and a peak at 1001.4 cm^{-1} was observed (Fig. 30).

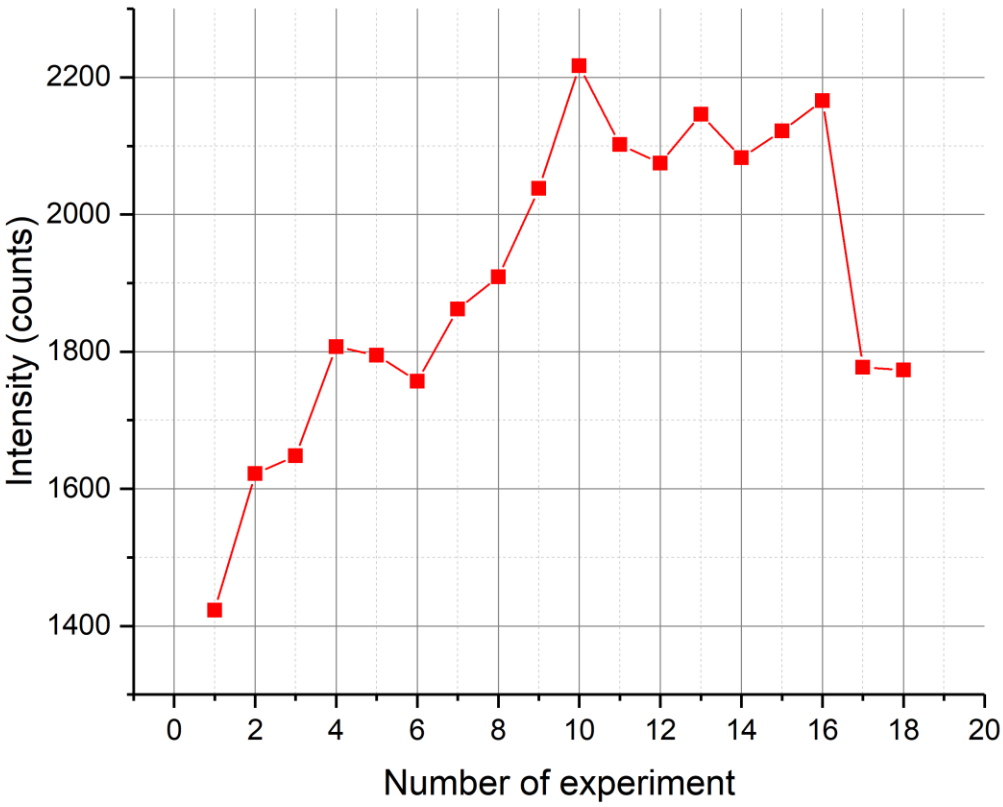

Fig. 30: 1001.4 cm^{-1} dynamics of intensity depending on the number of the experiment.

As can be seen from the graph, the number of particles increased in the first 10 spectra, then it did not change, and fell in the last two. In fact, it is difficult to say whether a change in the number of particles in a trap really affects a given distribution, and not other factors such as the focal point or a strong background.

7.5 Discussion

The experiments described in the previous section show that the Raman tweezer microspectroscopy is a possible technique for characterization of optically trapped nanoparticles. Optical trapping and Raman spectroscopy work well in combination handling nanoparticles one at a time and by clusters.

This work is a preparation for characterization weak Raman scutterers like EVs. Due to this strong Raman scatterers with clearly distinguishable peaks have been used in the experiments.

The optical trap works great for large particles 5-7 micrometers in diameter. It was not possible

to capture single particles of smaller size into the trap. Therefore, the results were exposed to Brownian motion, as can be seen in Fig. 30, and were also seen during experiments on the CCD camera from the imaging system. Where it was observed how the particles randomly hit the edge of the trap and flew out of it. It requires a significant decrease in the concentration of particles in the solution to be able to trap a single particle.

The Raman spectra obtained for large particles turned out to be inconsistent. It was not possible to distinguish chemical components for these particles. A possible reason may be a large proportion of the background radiation from the substrate and incorrect alignment. Replacing the substrate with microscope slides made of calcium fluoride can solve the problem, since CaF_2 contributes less in background than borosilicate glass and quartz. The alignment method described in section 5.2 can be improved by reducing the power of the lasers with ND filters so that the laser beams are a few pixels in size and thus can be aligned better.

For small particles, the Raman spectra were satisfying. They have a good signal-to-noise ratio. All polystyrene peaks from 600 to 1600 nm^{-1} were distinguishable.

The set-up showed overall stability and effectiveness for Raman spectroscopy and optical trapping. Although, there is a room for improvement. For example, replacement of the translational stage of the microscope objective 10 (Fig. 10) with a piezo-electric one could bring better precision of focusing. It is also possible to better efficiency of optical coupling 18-19 (Fig. 10) by improving the mobility of the translational stages on which it is located on. Beam collimation can be enhanced with a better beam expander 4-5 (Fig. 10). The sleeve of the imaging system must be reduced in length to overcome aberrations. The light from LED 15 (Fig. 10) should be isolated from the rest of the set-up, as it enters the spectrometer and contribute to the signal background.

8 Conclusion and future work

The Raman Tweezer Microspectroscopy is a strong method to use for characterization of a single EV or a small number of EVs or other bio-particles in an aqueous environment in the challenging size range near 200 nm. In this work the setup to carry out such experiments was designed and constructed. aligned and tasted on polystyrene nanoparticles for a further use for characterization of EVs. In this work the setup was constructed, aligned and tasted on polystyrene beads different sizes for a further use of characterization of EVs.

In the course of this work, the basic theoretical principles of Raman spectroscopy and microscopy in general were studied. Namely, the fundamentals of Raman scattering and the operation of optical tweezers were understood. Theoretical and practical principles of operation of a diffraction spectral device were also mastered.

The setup was designed in such a way as to use the equipment for both capture particles in an optical trap and excite Raman scattering. The microscope used in this study contained a water-immersive objective lens with high numerical aperture to increase the force of the optical radiation pressure of the visible range powerful laser beam to trap single nanoparticles and clusters. A grating based spectrometer was used to image the Raman signal from a sample. All these parts were combined in a microscope and optimized for Raman experiments. The physical and engineering foundations of spectroscopy and microscopy were studied.

Raman spectra were obtained of nanometer-sized polystyrene particles trapped by a laser tweezer. It provided sufficient sensitivity for the Raman measurement of the trapped nanoparticles. The confocal arrangement in the system eliminates the Raman signal of the water under the objective lens. The RTM provided a Raman spectrum of polystyrene beads about 200 nm in diameter with an exposure time of 1 second and allowed us to determine its molecular structure.

All the presented results have a potential for improvements. Unit design can be improved for better stability and overall efficiency. The set-up can also be optimized for a simpler alignment and increased signal output. For correct operation, it is necessary to get rid of clusters by reducing the concentration of particles in the sample. Background correction techniques need to be improved. one way is to replace cover slips from borosilicate glass and quartz to CaF_2.

With all the improvements the Raman tweezer microscope can be used for characterization of EVs.

Works cited

1. van Niel, G., G. D'Angelo, and G. Raposo, Shedding light on the cell biology of extracellular vesicles. Nature Reviews Molecular Cell Biology, 2018. **19**(4): p. 213-228.
2. Jamaly, S., et al., Impact of preanalytical conditions on plasma concentration and size distribution of extracellular vesicles using Nanoparticle Tracking Analysis. Scientific Reports, 2018. **8**.
3. Kruglik, S.G., et al., Raman tweezers microspectroscopy of circa 100 nm extracellular vesicles. Nanoscale, 2019. **11**(4): p. 1661-1679.
4. Tatischeff, I., et al., Fast characterisation of cell-derived extracellular vesicles by nanoparticles tracking analysis, cryo-electron microscopy, and Raman tweezers microspectroscopy. J Extracell Vesicles, 2012. **1**.
5. Enciso Martinez, A., EV TRAPPING: Raman characterization of single tumor-derived extracellular vesicles. . 2020, University of Twente.
6. Enciso-Martinez, A., et al., Label-free identification and chemical characterisation of single extracellular vesicles and lipoproteins by synchronous Rayleigh and Raman scattering. Journal of Extracellular Vesicles, 2020. **9**(1).
7. Rikkert, L.G., et al., Cancer-ID: Toward Identification of Cancer by Tumor-Derived Extracellular Vesicles in Blood. Frontiers in Oncology, 2020. **10**.
8. Enciso-Martinez, A., et al., Synchronized Rayleigh and Raman scattering for the characterization of single optically trapped extracellular vesicles. Nanomedicine-Nanotechnology Biology and Medicine, 2020. **24**.
9. Ferraro, J.R. & Nakamoto, K. & Brown, C.W., Introductory Raman Spectroscopy: Second Edition., Introductory Raman Spectroscopy: Second Edition, 2013.
10. Rosasco, G.J.. (1980). Raman microprobe spectroscopy. Advances in Infrared and Raman Spectroscopy. 7. 223-282.
11. Ashkin A., Acceleration and Trapping of Particles by Radiation Pressure, Phys. Rev. Lett., 1970. **24**: p. 156–159.
12. Neuman, K.C. and S.M. Block, Optical trapping. Review of Scientific Instruments, 2004. **75**(9): p. 2787-2809.
13. Bradac, C., Nanoscale Optical Trapping: A Review. Advanced Optical Materials, 2018. **6**(12).
14. Marago, O.M., et al., Optical trapping and manipulation of nanostructures. Nature Nanotechnology, 2013. **8**(11): p. 807-819.
15. Loudon, Rodney. Quantum Theory of light. Oxford, Clarendon Press, 1973.
16. Harada Y, Asakura T (1996). "Radiation Forces on a dielectric sphere in the Rayleigh Scattering Regime". Optics Communications. **124** (5–6): 529–541.
17. Yakovlev V., Electrodynamics lecture notes from Novosibirks State University, 2009.
18. HÜBNER Photonics Company, Cobolt 05-01 Series, Flamenco 660 nm datasheet, 2022.
19. Olympus Corporation, EVIDENT, UPLSAPO60XW datasheet, objective datasheet, 2022.
20. Teledyne Prinston Instruments, IsoPlane datasheet, Rev C4, 2022, https://www.princetoninstruments.com/wp-content/uploads/2021/07/IsoPlane-Rev-C4-28-01-2022.pdf

21. 1951 USAF resolution test chart, wikipedia the free encyclopedia, https://en.wikipedia.org/wiki/1951_USAF_resolution_test_chart.
22. Mazilu, Michael & De Luca, Anna Chiara & Riches, Andrew & Herrington, C & Dholakia, Kishan. (2010). Optimal Algorithm for Fluorescence Suppression of Modulated Raman Spectroscopy. Optics express. 18. 11382-95. 10.1364/OE.18.011382.
23. Ajito, Katsuhiro & Torimitsu, Keiichi. (2002). Single Nanoparticle Trapping Using a Raman Tweezers Microscope. Applied Spectroscopy. 56. 541-544. 10.1366/0003702021955015.
24. Wu, My., Ling, Dx., Ling, L. *et al.* Stable optical trapping and sensitive characterization of nanostructures using standing-wave Raman tweezers. *Sci Rep* **7**, 42930 (2017).
25. Thorlabs, Inc. (2019). *EDU-OT2 EDU-OT2/M Portable Optical Tweezers. User Guide.* Newton, New Jersey. MA: Author.